# Molecular Beam Scattering from Supercooled Sulfuric Acid: Collisions of HCl, HBr, and $HNO_3$ with 70 wt % $D_2SO_4$

**John R. Morris,[†] Peter Behr,[‡] Melissa D. Antman,[§] Bradley R. Ringeisen, Jennifer Splan, and Gilbert M. Nathanson***

*Department of Chemistry, University of Wisconsin-Madison, 1101 University Avenue, Madison, Wisconsin 53706*

*Received: January 7, 2000; In Final Form: May 23, 2000*

Proton exchange, residence time, and gas uptake measurements are used to explore collisions and reactions of HCl, HBr, and $HNO_3$ with 70 wt % $D_2SO_4$ at 213 K. These studies help to provide a detailed picture of HX (X = Cl, Br, $NO_3$) energy transfer to sulfuric acid and the fate of the HX molecules immediately after thermalization at the $D_2O/D_2SO_4$ surface. We find that the three molecules readily dissipate their excess kinetic energy and become trapped momentarily in the interfacial region. However, only 11 ± 3% of the thermalized HCl and 22 ± 3% of the thermalized HBr molecules undergo H → D exchange; the HCl and HBr that do not react are found to desorb from the acid within $2 \times 10^{-6}$ s. In contrast, more than 95% of the initially trapped $HNO_3$ molecules are converted to $DNO_3$. The HX molecules that undergo exchange dissolve within the deuterated acid for characteristic times of $5 \times 10^{-5}$ s (HCl), $3 \times 10^{-3}$ s (HBr), and $1 \times 10^{-1}$ s ($HNO_3$) before they desorb thermally as DX. The scattering experiments imply that the desorption of thermalized HCl and HBr molecules is, on average, faster than their solvation and reaction in the interfacial and bulk regions of 70 wt % $D_2SO_4$. Although $HNO_3$ is less acidic than HCl or HBr, it appears to hydrogen bond more strongly to surface $D_2O$ and $D_2SO_4$, enabling it to be captured by the acid in nearly every collision.

## Introduction

Heterogeneous reactions of gas-phase molecules with sulfuric acid aerosols play a significant role in the chemistry of the stratosphere.[1,2] These heterogeneous processes include the production of halogen molecules from the aerosol-catalyzed reactions of HCl and HBr with $ClONO_2$, $BrONO_2$, HOCl, and HOBr, particularly in colder regions of the stratosphere where HCl and HBr are more soluble in the water-rich aerosols.[3−7] Additionally, the absorption of $HNO_3$ into the supercooled acid removes nitrogen oxides from the stratosphere and can alter the freezing, growth, and catalytic properties of the aerosols.[8] Our objective is to probe the nature of the initial gas-sulfuric acid collision and the immediate fate of the HCl, HBr, and $HNO_3$ molecules trapped at the acid's surface as they either desorb into the gas phase or react in the interfacial or bulk regions of the acid. We perform these studies by exposing deuterated sulfuric acid (70 wt % $D_2SO_4$ at 213 K) to molecular beams of the three protic gases. The exiting species are monitored by mass spectroscopy and time-of-flight (TOF) velocity analysis in order to separate nonreactive collisions from those that involve H → D exchange. The supercooled 70 wt % acid is typical of aerosol concentrations in the mid-latitude region of the lower stratosphere.[2]

The different channels open to HX molecules (X = Cl, Br, $NO_3$) when they collide with deuterated sulfuric acid are outlined in Figure 1.[9] The initial impact governs whether the incoming molecule scatters away from the surface (direct inelastic scattering) or whether it dissipates its excess energy through one or several bounces and binds momentarily to interfacial $D_2O$ or $D_2SO_4$ (thermalization and trapping). Molecules that become trapped at the interface may be propelled back into the gas phase by the thermal motions of the surface atoms (trapping−desorption). Alternatively, if HX molecules form strong hydrogen bonds to surface OD or SO groups, they may become sufficiently solvated to dissociate into $H^+$ and $X^-$ in the interfacial region or to be transported more deeply into the acid before ionization occurs. At high acid concentrations, HX may undergo attack by $D^+$ or transfer H or X atoms to solvent species in a concerted reaction.

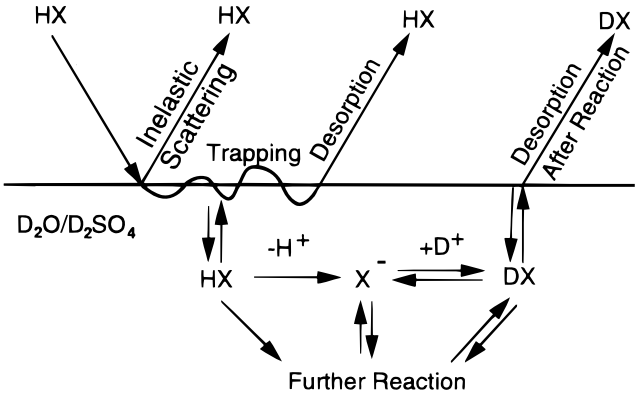


**Figure 1.** Observed pathways for an acidic molecule HX colliding into deuterated sulfuric acid. Reactions between HX and the acid can occur in the interfacial or bulk regions.

The studies described below indicate that all HX product species ($X^-$, DX, $HXD^+$, $XSO_3^-$) ultimately leave the acid as thermally desorbing DX molecules. The reactivity of HX

* Author to whom correspondence should be addressed.

[†] Present address: Department of Chemistry, Virginia Polytechnic Institute and State University, Blacksburg, VA 24061.

[‡] Present address: Department of Physical and Theoretical Chemistry, University of Essen, Essen, Germany.

[§] Present address: Pharmacia Corp., Kalamazoo, MI 49001.

10.1021/jp000105o CCC: $19.00 
Published on Web 07/01/2000

**TABLE 1: Selected Properties of 72 wt % $H_2SO_4$ at 213 K**

| | |
|---|---|
| equivalent $D_2SO_4$ wt % | 70.2 |
| mole ratio | 2.1:1 $H_2O$:$H_2SO_4$ |
| molarity | 12.4 M |
| Hammett acidity | −6.1 |
| $K_{dissoc}$ ($HSO_4^-/DSO_4^-$) at 25 °C | $1.0 \times 10^{-2}/4.5 \times 10^{-3}$ |
| $\Delta H_{vap}$ ($H_2O$) | 55 kJ/mol |
| $P_{vap}$ (all $H_2O$) | $1.3 \times 10^{-4}$ Torr |
| viscosity | 3100 cP |
| surface tension | >74 dynes/cm |
| approximate composition[a] | |
| $H_3O^+$ | 33% |
| $HSO_4^-$ | 32% |
| $SO_4^{2-}$ | <1% |
| $H_2O$ | 35% |

[a] Ref 17, assuming that $H^+$ is present as $H_3O^+$.

molecules impinging on the acid is, therefore, proportional to the DX desorption intensity. We define $f_{exch}$ as the fraction of thermally equilibrated HX molecules that undergo H → D exchange. This fraction is directly observable in our experiments through measurements of the relative fluxes of thermally desorbing HX and DX molecules, and it provides a reactivity scale for HX with sulfuric acid solvent. $f_{exch}$ should also provide an upper limit to the heterogeneous reaction probability of HX with other solvated atmospheric molecules in the case in which HX reacts with the acid before it reacts with the solute molecule. Within this constraint, *$f_{exch}$ yields the fraction of thermalized HX molecules that are available for solute−solute reactions in sulfuric acid*. In addition to these H → D exchange measurements, we use pulsed molecular beams to compare the residence times of HX molecules that undergo trapping−desorption and those that undergo exchange. These experiments provide information on the different time scales and locations of thermalization and solvation.

The initial interactions between HX and $D_2SO_4$ depend on the composition and structure of the interfacial region of the acid. This region has been investigated by surface tension,[10] sum frequency generation (SFG),[10,11] and Auger electron spectroscopy[12] for $H_2SO_4$ solutions. The surface tension and Auger studies indicate that there is little segregation of the lower-surface-free-energy $H_2SO_4$ to the surface of the acid, implying that the interfacial composition of 70 wt % $D_2SO_4$ should be close to the 2.1:1 $D_2O$:$D_2SO_4$ ratio in the bulk. The outermost $D_2O$ and $D_2SO_4$ species are likely to be in their neutral state because of incomplete solvation of $D_3O^+$ and $DSO_4^-$ ions at the surface, although tightly bound ion pairs may also be present. Judging from SFG studies of $H_2SO_4$, we expect that interfacial OD and SO groups should form a deuterium-bonding network in which no free OD groups project outward from the surface.

The fate of molecules that diffuse into solution is governed by the bulk interactions of HX with sulfuric acid. Selected properties of 72 wt % $H_2SO_4$ at 213 K (equivalent to 70.2 wt % $D_2SO_4$ at the same 0.32 mole fraction) are listed in Table 1. Both $H_2SO_4$ and $D_2SO_4$ solutions are highly viscous,[13] low-vapor-pressure[14] liquids at 213 K, supercooled by ∼20 K for the hydrogen isotope. The Hammett acidities, which are extensions of the pH scale to strong acids, are −6.1 for each acid, indicative of their strongly acidic character.[15] Raman measurements show that 72 wt % $H_2SO_4$ at 25 °C is extensively ionized, with little or no molecular $H_2SO_4$ present.[16] Thermodynamic calculations[17] predict that this acid is composed of nearly equal fractions of $H_3O^+$, $HSO_4^-$, and $H_2O$ at 213 K (assuming that $H^+$ is present as $H_3O^+$).[17] The equal Hammett acidities and comparable dissociation constants[18] for $DSO_4^-$ and $HSO_4^-$ suggest that 70 wt % $D_2SO_4$ and 72 wt % $H_2SO_4$ have similar compositions.

**TABLE 2: Selected Properties of HCl, HBr, and $HNO_3$**

| | HCl | HBr | $HNO_3$ |
|---|---|---|---|
| ppbv in stratosphere[a] | 0−3 | 0−0.01 | 1−10 |
| mass (amu) | 36.5 | 80.9 | 63.0 |
| polarizability (Å$^3$) | 2.7 | 3.6 | |
| dipole moment (*D*) | 1.1 | .83 | 2.2 |
| boiling point (°C) | −85 | −67 | 83 |
| dissociation constant, $K_a$ | $\sim 10^{6-7}$ | $\sim 10^{8-9}$ | ∼20 |
| $\Delta H_{vap}$[b] ($H_2O$, 25° C) (kJ/mol) | 75 | 85 | 71 |
| $\Delta H_{vap}$[c] (72 wt % $H_2SO_4$, 213 K) (kJ/mol) | ∼30 | ∼42 | ∼56 |
| $H^*$[c](72 wt % $H_2SO_4$, 213 K) (M/atm) | $1 \times 10^2$ | $2 \times 10^4$ | $3 \times 10^6$ |
| $D$[d](72 wt % $H_2SO_4$, 213 K) (cm$^2$/s) | $5 \times 10^{-9}$ | $5 \times 10^{-9}$ | $4 \times 10^{-9}$ |
| predicted residence time $\tau$ (s)[e] | $1 \times 10^{-7}$ | $2 \times 10^{-3}$ | 0.2 |

[a] Ref 2. [b] Enthalpy of vaporization from water at 25 °C [c] Solubilities and enthalpies estimated from vapor pressures in ref 17. [d] Liquid-phase diffusion coefficient from ref 55. [e] Calculated from $H^*$, $D$, and eq 2 using the measured $f_{exch} \approx \alpha_{th}$. See text and refs 40, 42, and 63.

The solubilities of HCl, HBr, and $HNO_3$ in sulfuric acid have been determined by vapor pressure,[19] Knudsen cell,[20] flow tube,[4,21] and droplet train[6] measurements and are in generally good agreement with thermodynamic calculations.[17] For concentrations near 72 wt % $H_2SO_4$ at 213 K, the effective Henry's law solubilities, H*, are estimated to range from $1 \times 10^2$ M/atm for HCl and $2 \times 10^4$ M/atm for HBr to $3 \times 10^6$ M/atm for $HNO_3$.[17] Robinson et al. find that the solubility of HCl in 69 wt % $H_2SO_4$ is greater than predicted by calculations, perhaps because of the reaction of HCl with $H_2SO_4$ to form $ClSO_3H$.[6] Our experiments support enhanced HCl solubility in ∼70 wt % sulfuric acid.

Table 2 shows that each HX molecule is predicted to dissolve exothermically in 72 wt % $H_2SO_4$ at 213 K,[17] although the values are smaller than those for dissolution in pure water at 25 °C. Raman measurements indicate that nitric acid exists as 97% $HNO_3$ and 3% $NO_3^-$ in 72 wt % $H_2SO_4$ at 25 °C, with no reported $H_2NO_3^+$ or $NO_2^+$.[22] The extent of dissociation of HCl and HBr in sulfuric acid solutions has not been measured, but the much larger dissociation constants of these molecules[23] make it plausible that they ionize substantially more than $HNO_3$. The hydrogen bonding strengths of the three gases to $H_2O$ and $H_2SO_4$ appear to follow a trend opposite to their acidity: quantum calculations predict that the HX−$H_2O$ dissociation energies vary from ∼16 and ∼19 kJ/mol for HBr and HCl, respectively, to ∼31 kJ/mol for $HNO_3$.[24−28] The HX−$H_2SO_4$ bonds are 20% to 40% stronger.[29]

The experiments described below are used to explore the differences in energy transfer, proton exchange rates, and residence times of HCl, HBr, and $HNO_3$ in contact with 70 wt % $D_2SO_4$ at 213 K. We find that 95% of the $HNO_3$ molecules that are trapped at the surface of the acid dissolve for an average time of 0.1 s, undergoing H → D exchange before desorbing. In contrast, nearly 90% of the thermalized HCl and 80% of the thermalized HBr desorb within 2 $\mu$s from the interface, escaping reaction. The experiments suggest that HCl and HBr impinging on 70 wt % sulfuric acid behave more often like nonreactive gases than carriers of Cl and Br into solution.

## Experiment

The molecular beam scattering apparatus is depicted in Figure 2. The machine consists of a doubly differentially pumped molecular beam chamber, a scattering chamber that contains the liquid sample and two chopper wheels, and a doubly differentially pumped chamber housing a quadrupole mass

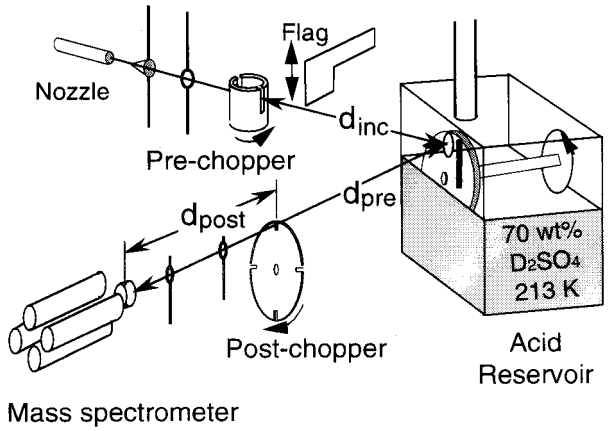


**Figure 2.** Schematic diagram of the scattering apparatus. The reservoir containing the acid is sealed, except for a 0.88-cm-diameter hole centered at the interaction region.

**TABLE 3: Selected Molecular Beam Conditions and Experimental Results**

| incident gas | $E_{inc}$ (kJ/mol) | $\langle \Delta E_{IS} \rangle / E_{inc}$ | $\pm \sigma_{IS}/E_{inc}$[c] | IS:TD (for HX)[d] |
|---|---|---|---|---|
| 2% HCl in $H_2$ | 105 | 0.75 | ±0.14 | 0.74:0.26 |
| 5% HCl in He | 47 | 0.70 | ±0.15 | 0.40:0.60 |
| 10% HCl in $N_2$ | 14 | – | – | <0.1:>0.9 |
| 2% HBr in $H_2$ | 145 | 0.81 | ±0.13 | 0.70:0.30 |
| 2% HBr in $H_2$[a] | ≈115 | – | – | 0.5:0.5 |
| 1% $HNO_3$ in $H_2$[b] | 170 | 0.85 | ±0.09 | >0.9:<0.1 |
| 2% Ar in $H_2$ | 105 | 0.70 | ±0.09 | 0.88:0.12 |
| 2% Kr in $H_2$ | 125 | 0.79 | ±0.12 | 0.86:0.14 |

[a] $E_{inc}$ lowered and broadened by reduction of backing pressure from 760 to 200 Torr. [b] $E_{inc}$ = 150 kJ/mol for the incident $HNO_3$ in Figure 6. [c] Ratio of width of IS component to incident beam energy. [d] The ratios include both HX and DX desorption for HCl and HBr.

spectrometer. The mass spectrometer is oriented at 90° with respect to the incident beam.

Molecular beams of HCl, HBr, and $HNO_3$ are created by expanding mixtures of each species with a carrier gas through a 0.09-mm-diameter glass nozzle at ~750 Torr total pressure. The beam energies are controlled by the backing pressure, nozzle temperature, and mass ratio of the carrier gas to reagent gas. The conditions for each HX beam are listed in Table 3. The nozzle is heated to 80 °C to suppress HX dimerization and generate incident beams that ionize in the mass spectrometer to yield monomer ion/dimer ion ratios, $HX^+/H_2X^+$, that are greater than 20:1 for HCl and HBr and greater than 6:1 for $HNO_3$. The incident HX fluxes are estimated to be below $10^{15}$ $cm^{-2}$ $s^{-1}$ (effective pressures below $3 \times 10^{-9}$ atm).

Solutions near 70 wt % $D_2SO_4$ are prepared by diluting 99 wt % $D_2SO_4$ (Aldrich) with $D_2O$. A 50-mL sample is degassed for 30 min before transfer to a Teflon reservoir located inside the scattering chamber. The temperature is then lowered to $T_{acid}$ = 213 ± 1 K by circulating chilled methanol through Teflon-coated cooling lines that pass through the acid.[30] Titrations show that the acid concentration rises by <0.2 wt % per week through $D_2O$ evaporation. The HCl and HBr H → D exchange experiments were carried out with acid near 69.5 wt % $D_2SO_4$, whereas the HCl and HBr residence times were measured in 68.6 wt % $D_2SO_4$. The $HNO_3$ exchange and residence time measurements were made using 70.5 wt % $D_2SO_4$. We found that freezing rarely occurred at 213 K at these concentrations.

Continuously renewed films of acid are created in a vacuum by partially immersing a 5.0-cm-diameter vertical glass wheel in the acid.[31] As the wheel rotates, it picks up a layer of liquid, and a cylindrical Teflon blade removes the outer portion of the film, leaving behind a clean ~0.2-mm-thick layer. The top portion of the wheel passes behind a 0.88-cm-diameter hole in the reservoir, which is positioned at the center of the scattering chamber. The 0.78-cm-diameter molecular beam strikes the acid through this hole at an incident angle, $\theta_{inc}$, of 45°. The exposure time of the liquid to the molecular beam, $t_{exp}$, is varied from 0.046 to 0.46 s by rotating the glass wheel from 1.7 to 0.17 Hz.

The Teflon reservoir is sealed, except for the 0.88-cm hole, to suppress $D_2O$ evaporation, allowing the chamber pressure to be maintained below $2 \times 10^{-6}$ Torr by a water-baffled diffusion pump. From the vapor pressure of $10^{-4}$ Torr for 72 wt % $H_2SO_4$ at 213 K, we estimate that water molecules desorbing from the acid should deflect fewer than 5% of the impinging molecules from striking the surface.[32] The change in evaporative flux of $D_2O$ from the acid can be used to monitor changes in film composition as water desorbs from the acid-coated wheel. We find that there is no measurable change in the amount of $D_2O$ that desorbs from the acid as the exposure time is varied from 0.046 to 0.46 s. This steady $D_2O$ flux demonstrates that the $D_2O/D_2SO_4$ concentration within the patch of acid that is exposed to the vacuum remains constant during these times.

Molecules scattering or desorbing from the acid are detected by a mass spectrometer at an exit angle, $\theta_{fin}$, of 45°.[33] TOF measurements are made by employing either "post-chopper" or "pre-chopper" wheels to modulate the scattered or incident molecules, respectively. In the post-chopper configuration, molecules strike the acid continuously. The exiting molecules are chopped into 20-$\mu$s gas pulses (fwhm) by an 18-cm-diameter, post-chopper wheel with four 1.6-mm slots rotating at 150 Hz, as shown in Figure 2. A multichannel scaler with 2-$\mu$s bins is used to record the mass spectrometer signal as a function of arrival time over an 18.2 ± 0.1 cm flight path, $d_{post}$. In this configuration, the TOF spectra are determined solely by the velocities of the scattered and desorbed molecules and are not related to the residence times of the gas molecules in solution. However, modulation of the incident beam before the molecules reach the acid provides a direct measurement of the amount of time they spend in contact with the acid before desorbing. As shown in Figure 2, these pre-chopper TOF spectra are recorded using a 2.5-cm-diameter cylindrical chopper with two 1.6-mm slots.[34] The chopper produces 65−50-$\mu$s pulses by spinning at 200−250 Hz.[35] In this configuration, the arrival time of a molecule is the sum of its incident and scattered gas-phase flight times and the time it spends in contact with the acid.

## Results and Analysis

**Post-Chopper Measurements of H → D Exchange.** The post-chopper spectra are plots of the mass spectrometer signal versus the flight time for molecules to traverse the distance $d_{post}$ at $\theta_{inc} = \theta_{fin} = 45°$. All spectra are corrected for electronic and timing offsets. The signal is proportional to the number density, $N(t)$, and is used to calculate the relative flux or probability, $P(E_{fin})$, that a molecule will scatter with translational energy $E_{fin}$. The energy distributions are computed from the relations $P(E_{fin}) \sim N(t)t^2$ and $E_{fin} = (1/2)m_{gas}(d_{post}/t)^2$.[32]

Figures 3a and 4a show TOF spectra for high-energy HCl ($E_{inc}$ = 100 kJ/mol) and HBr ($E_{inc}$ = 145 kJ/mol) scattering from 69.5 wt % $D_2SO_4$ at 213 K. The exposure time of the acid to the incident HX beams is $t_{exp}$ = 0.46 s. Detection at $m/e$ = 38 ($H^{37}Cl$) and $m/e$ = 82 ($H^{81}Br$) ensures that neither $D^{35,37}Cl$ nor $D^{79,81}Br$ isotopes contribute to the TOF spectra.

The open circles show that HCl and HBr scatter in a bimodal distribution. The molecules are observed to undergo direct inelastic scattering (IS), as evidenced by the sharp peak at early arrival times (high recoil energies), and thermal desorption (TD) at later arrival times (lower final energies). As discussed later, this TD component is attributed to molecules that dissipate their energy fully and become momentarily bound at the surface (trapped) before desorbing. The translational energy distributions in Figures 3b and 4b are separated into IS and TD contributions by assigning the TD distribution to the component of $P(E_{fin})$ that falls within a Boltzmann distribution, $P_{TD}(E_{fin}) = E_{fin}(RT_{acid})^{-2} \exp(-E_{fin}/RT_{acid})$.[32] The TD fits are represented by dashed lines in subsequent figures. The IS contribution is assigned to the difference between $P(E_{fin})$ and $P_{TD}(E_{fin})$, constrained such that $P_{IS}(E_{fin}) = 0$ at $E_{fin} = RT_{acid} = 1.8$ kJ/mol at 213 K. The fractional energy transfers in the IS channel and the IS:TD intensity ratios are summarized in Table 3. The HCl and HBr energy transfers in the inelastic channel are 70% or greater, whereas the IS:TD ratios rise steadily with increasing collision energy.

The TOF distributions for HCl and HBr molecules that have undergone H → D exchange to DCl and DBr are shown by the squares in Figures 3a and 4a. The total number of molecules that desorb thermally from the acid at $\theta_{fin} = 45°$ is proportional to the integrated thermal-desorption intensity for HX plus that for DX, specifically, $TD_{HX} + TD_{DX} = \int P_{TD}^{HX}(E_{fin})\, dE_{fin} + \int P_{TD}^{DX}(E_{fin})\, dE_{fin}$. The fraction of thermally equilibrated molecules that emerge as proton-exchanged DX is $f_{exch} = TD_{DX}/(TD_{DX} + TD_{HX})$. The small DCl and DBr signals in Figures 3 and 4, combined with six additional measurements for each gas, yield average values of $f_{exch}$ equal to $0.11 \pm 0.03$ and $0.22 \pm 0.03$, respectively. The error bars reflect a $\pm 0.01$ uncertainty in reproducibility and an estimated $\pm 0.02$ uncertainty in fitting the thermal-desorption components. These low $f_{exch}$ values demonstrate that nearly 90% of the HCl molecules and 80% of the HBr molecules that thermally accommodate in the interfacial region desorb into the vacuum before they undergo H → D exchange.

The calculation of $f_{exch}$ from HX and DX TOF spectra relies on two conditions. All HX and DX molecules must desorb from the acid during the measurement time (zero net uptake) in order to avoid corrections for any HX or DX molecules remaining in the acid. Uptake measurements reported below confirm that the net uptake is close to zero for both HCl and HBr. Additionally, the angular distributions of the thermally desorbing HX and DX must be the same in order for measurements at $\theta_{fin} = 45°$ to represent the total flux of desorbing molecules. Although measurements were not made at angles other than $\theta_{fin} = 45°$, the uptake measurements, which integrate over all exit angles, support the TOF calculations of $f_{exch}$.

The overall net uptake of HCl ($E_{inc} = 14$ kJ/mol) and HBr ($E_{inc} = 145$ kJ/mol) were determined by measuring the differences in mass spectrometer signals at $m/e = 35$ ($^{35}Cl^+$) and $m/e = 79$ ($^{79}Br^+$) when the beam is blocked by a Teflon flag and when the beam collides directly with the acid for a time $t_{exp}$, as determined by the rotation speed of the acid-covered wheel. A reduction in signal is due to the net uptake of gas into the acid according to $S(t_{exp}) = (P_f - P_a)/(P_f - P_b)$, where $P_f$, $P_a$, and $P_b$ are the gas pressures when the incident molecules strike the flag, strike the acid, and are blocked from entering the scattering chamber, respectively.[36,37] $S(t_{exp})$ can range from 0 for no net uptake to 1 for complete uptake. The $m/e$ values at 35 and 79 were chosen because they do not discriminate between HCl and HBr parent molecules that scatter without reacting and

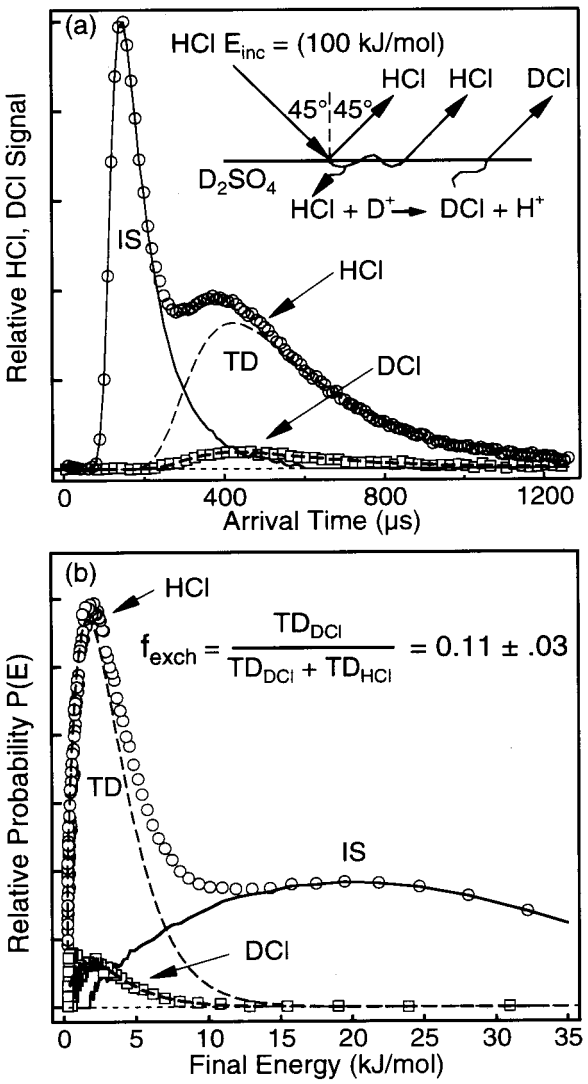


**Figure 3.** (a) Post-chopper time-of-flight (TOF) spectra of HCl (○) and DCl (□) exiting from 69.5 wt % $D_2SO_4$ at 213 K after collisions of HCl with the acid at 100 kJ/mol. "IS" and "TD" refer to inelastic scattering and thermal desorption. (b) Relative fluxes (probabilities) of HCl and DCl exiting from the acid versus final energy. The dashed lines are fits to a Boltzmann distribution at 213 K. $f_{exch}$ is the fraction of thermalized molecules that undergo H → D exchange.

those that undergo exchange in the acid and desorb as DCl and DBr. We measured the net uptake for $^{35}Cl$ and $^{79}Br$ to be $0.01 \pm 0.02$ and $0.00 \pm 0.02$, respectively, at $t_{exp} > 0.2$ s. Fewer measurements were performed at shorter exposure times, but the measured uptakes were found to be less than 0.01 for both HCl and HBr. Additionally, we could not detect changes in $f_{exch}$ at different exposure times. These results demonstrate that nearly all incident HCl (HBr) molecules escape from the acid either as parent HCl (HBr) or as proton-exchanged DCl (DBr) species.

Uptake measurements at $m/e = 36$ ($H^{35}Cl$), which monitor the conversion of HCl to DCl, provide an independent determination of $f_{exch}$ as $S(H^{35}Cl)/p_{trap}$, where $p_{trap}$ is the HCl trapping probability. The uptake at $m/e = 36$ was measured to be $S = 0.09$ at $E_{inc} = 14$ kJ/mol, but $p_{trap}$ is difficult to measure directly because most HCl molecules desorb immediately from the acid. Separate studies of HCl collisions with liquid glycerol, where HCl undergoes longtime solvation, yield a $p_{trap}$ value of 0.9 at $E_{inc} = 14$ kJ/mol.[38] If $p_{trap}$ is also close to 0.9 for 69.5 wt % $D_2SO_4$, as suggested by the TOF analysis below, then $f_{exch}$ is approximately 0.1 and within the uncertainty of $0.11 \pm 0.03$

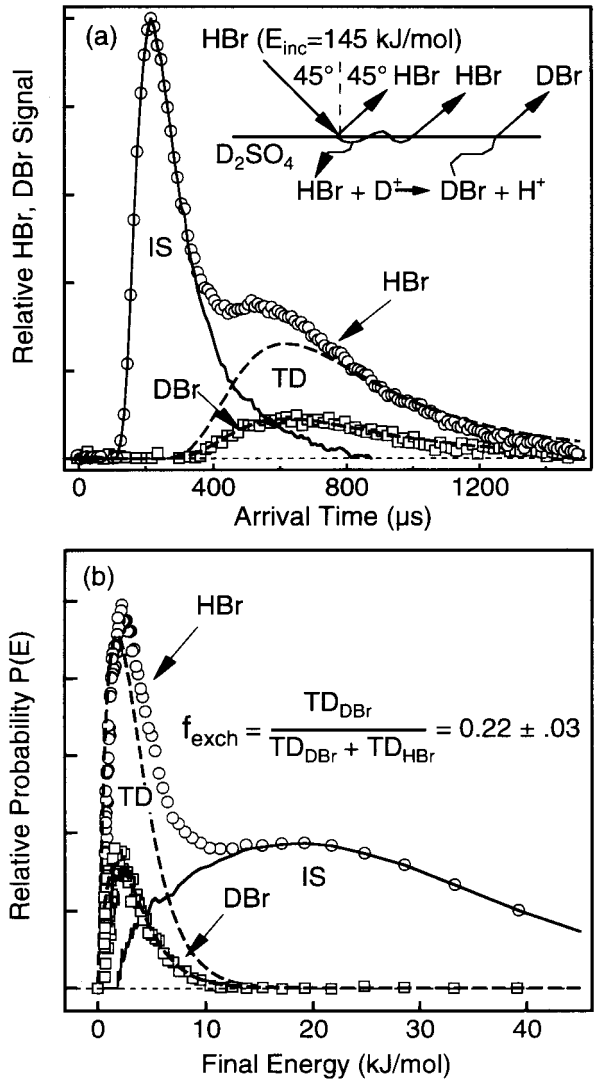


**Figure 4.** (a) TOF spectra of HBr (○) and DBr (□) exiting from 69.5 wt % $D_2SO_4$ at 213 K after collisions of HBr with the acid at $E_{inc}$ = 145 kJ/mol. (b) Relative probabilities of HBr and DBr exiting from the acid versus final energy.

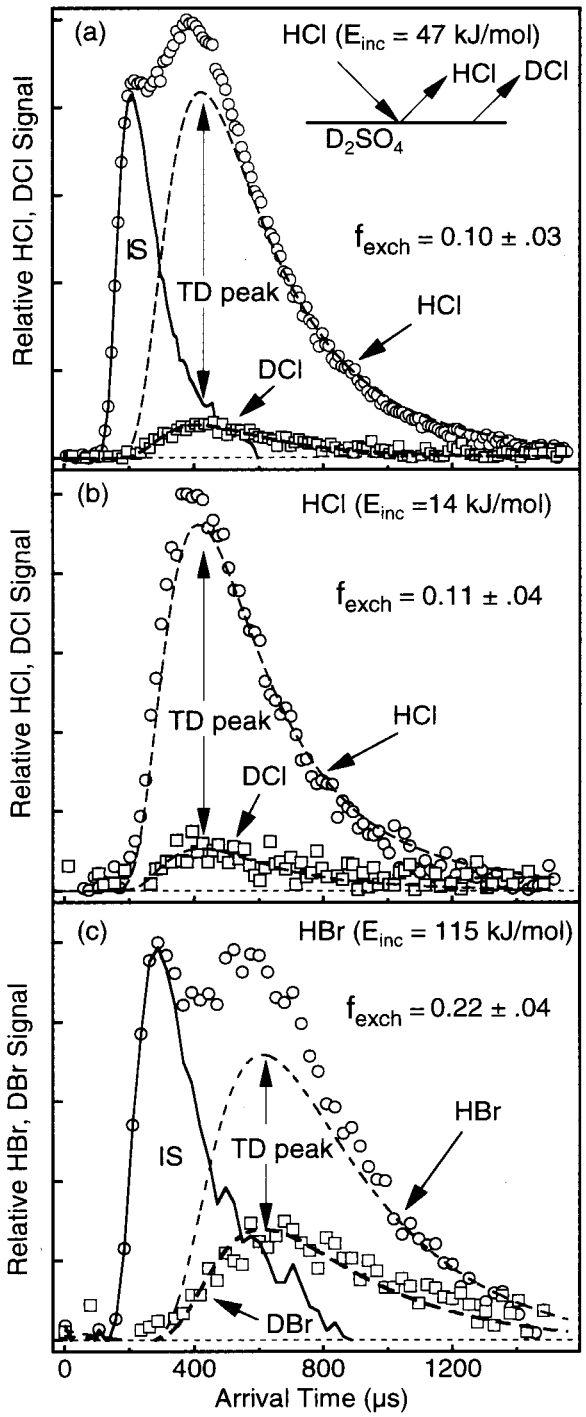


**Figure 5.** Measurements of $f_{exch}$ at different HCl and HBr incident energies. (a) TOF spectra of HCl (○) and DCl (□) at $E_{inc}$(HCl) = 47 kJ/mol. (b) TOF spectra of HCl (○) and DCl (□) at $E_{inc}$(HCl) = 14 kJ/mol. (c) TOF spectra of HBr (○) and DBr (□) at $E_{inc}$(HBr) = 115 kJ/mol.

derived from the TOF spectra. This agreement supports the assertion that the HX and DX species desorb with similar angular distributions.

We can gain further insight into the H → D exchange process by measuring $f_{exch}$ at different HCl and HBr collision energies. Figure 5 shows spectra recorded at lower energies of 47 and 14 kJ/mol for HCl and 115 kJ/mol for HBr. In each case, the DCl and DBr spectra are fit with Maxwell−Boltzmann distributions at the temperature of the acid. The leading edge of the HCl spectrum at 14 kJ/mol is due to directly scattered HCl molecules, which account for at most 10% of the signal intensity at $\theta_{fin}$ = 45°. A comparison of the HX and DX thermal desorption intensities reveals that $f_{exch}$ does not change with collision energy, even though the inelastic scattering contribution diminishes at lower $E_{inc}$. As discussed later, the thermal desorption of product DCl and the invariance of $f_{exch}$ with $E_{inc}$ imply that only thermalized HCl molecules undergo H → D exchange.

The use of $D_2SO_4$ may potentially skew the values of $f_{exch}$ through isotope effects on HX dissociation and DX recombination. The HX−$D_2SO_4$ system was selected over the DX−$H_2SO_4$ system because of the greater difficulty in generating stable molecular beams of DCl, DBr, and $DNO_3$ with little HX contamination. To gauge the effects of isotopic substitution, we scattered 100 kJ/mol DCl from 71 wt % $H_2SO_4$ and measured $f_{exch}$ to be 0.12. This measurement lies within the 0.11 ± 0.03 value for HCl reacting with 69.5 wt % $D_2SO_4$ (equivalent to 72.2 wt % $H_2SO_4$).

Figure 6 demonstrates that $HNO_3$ behaves very differently from HCl and HBr. The top panel shows that most parent $HNO_3$ ($m/e$ = 63) molecules either scatter inelastically or disappear into 69.5 wt % $D_2SO_4$; there is little evidence for thermal

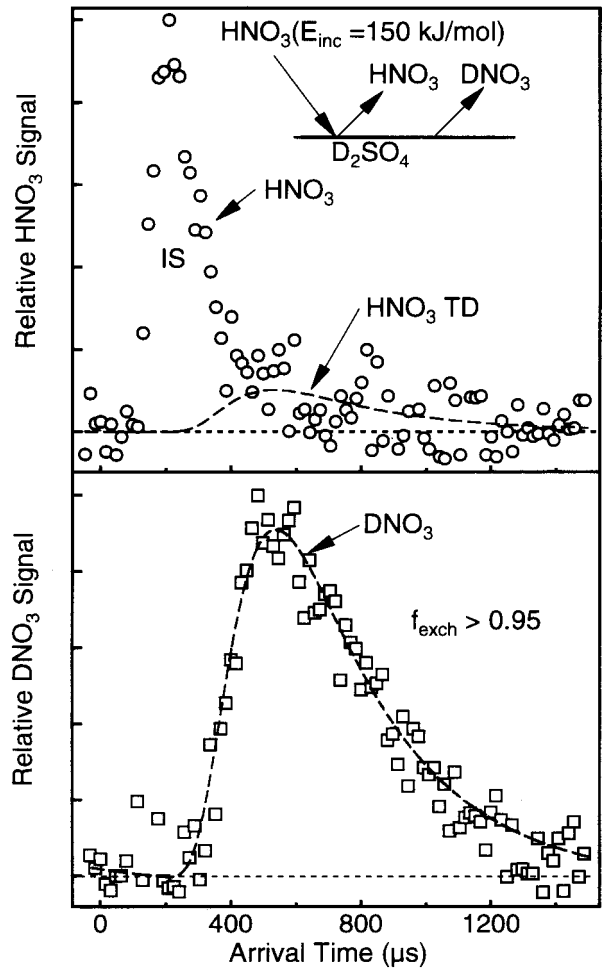


**Figure 6.** (a) TOF spectrum of $HNO_3$ exiting from 70.5 wt % $D_2SO_4$ at 213 K at $E_{inc}$ = 150 kJ/mol. (b) TOF spectrum of $DNO_3$, scaled to the signal in panel a. The weak $HNO_3$ TD signal indicates that H → D exchange of thermalized $HNO_3$ is nearly complete.

desorption of parent $HNO_3$. The dashed line is an estimate of the amount of $HNO_3$ that survives thermalization without undergoing H → D exchange. The bottom panel shows the signal for $m/e$ = 64 ($DNO_3$) for the same $HNO_3$ incident beam, plotted relative to the scattered $m/e$ = 63 signal. The intensity of the observable $DNO_3$ signal is at least 10 times that of the thermally desorbing $HNO_3$ in the upper panel. As described in the Appendix, we estimate that 36% of the $HNO_3$ molecules that enter the acid remain in solution and do not desorb as $DNO_3$ within the exposure and observation time of $t_{exp}$ = 0.46 s. This correction yields a value of $f_{exch}$ greater than 0.95. Thus, at least 9 out of 10 $HNO_3$ molecules that are initially trapped at the surface undergo H → D exchange before they desorb.

**Residence Time Measurements.** The pre-chopper TOF spectra can be used to determine residence (solvation) times for HX molecules that desorb from the acid as HX or as DX. These measurements provide approximate time scales for the trapping−desorption and trapping−reaction−desorption pathways.

The arrival times of a molecule in the TOF spectrum using the pre-chopper (pulsed) and post-chopper (continuous) molecular beams are (see Figure 2)

$$t_{arrival}(pre) = d_{inc}/v_{inc} + t_{res} + d_{pre}/v_{fin}$$

$$t_{arrival}(post) = d_{post}/v_{fin}$$

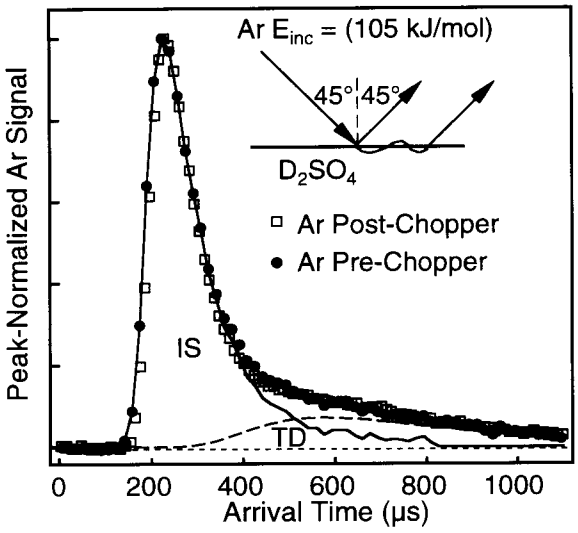


**Figure 7.** Comparison of post- and pre-chopper Ar spectra at $E_{inc}$ = 105 kJ/mol. The post-chopper arrival times have been scaled so that the flight paths for both spectra are equal to $d_{pre}$ = 24.4 cm. The nearly identical thermal desorption signals indicate that the Ar residence times are less than 2 $\mu$s.

where $d_{inc}$ = 5.0 cm and $d_{pre}$ = 24.4 cm are the distances from the pre-chopper to the acid and from the acid to the mass spectrometer, respectively; $d_{post}$ = 18.2 is the distance from the post-chopper to the mass spectrometer; $v_{inc}$ is the incident velocity of the molecule; and $v_{fin}$ is its velocity after it scatters or desorbs. The time $t_{res}$ is the time that the molecule spends in contact with the acid before desorbing.

The distribution of residence times is extracted from the pre-chopper spectrum using the following procedure. The HX post-chopper arrival times are first multiplied by $d_{pre}/d_{post}$ = 1.34 to set the flight paths equal to $d_{pre}$ = 24.4 cm for both pre- and post-chopper TOF spectra. The peak of the IS component of the HX pre-chopper spectrum is then shifted in time to match the IS peak of the HX post-chopper spectrum. This shift removes the $d_{inc}/v_{inc}$ time offset and sets the residence time for inelastically scattered molecules to zero, as expected for the sub-nanosecond duration of a direct collision. The peak intensities of the IS channels are then normalized to correct for the different duty cycles of the two-slotted pre-chopper and the four-slotted post-chopper wheels. The same time and intensity corrections are then applied to the DX pre- and post-chopper spectra. Any remaining differences in arrival times and intensities of thermally desorbing HX and DX in the pre-chopper and post-chopper spectra are due to the residence times of molecules in contact with the acid. As described in the Appendix, we are able to measure residence times greater than 2 $\mu$s with this procedure.

Figure 7 provides a test of the procedure by comparing pre- and post-chopper spectra for argon scattering at $E_{inc}$ = 105 kJ/mol from 69.5 wt % $D_2SO_4$. The two distributions are nearly identical at fast and slow arrival times. The overlap of the thermal-desorption components reflects the weak binding and submicrosecond residence times of thermally equilibrated argon atoms at the acid surface.

Figures 8a and 9a show post- and pre-chopper spectra for HBr and HCl, respectively, scattering at high collision energies from 68.6 wt % $D_2SO_4$. As for argon, the HBr and HCl TD components of the post- and pre-chopper spectra overlap extremely well. This overlap demonstrates that the residence times for thermally equilibrated HBr and HCl molecules that do not react are less than 2 $\mu$s. We also obtain good agreement at lower impact energies, as shown in Figure 9b; the 47 kJ/mol

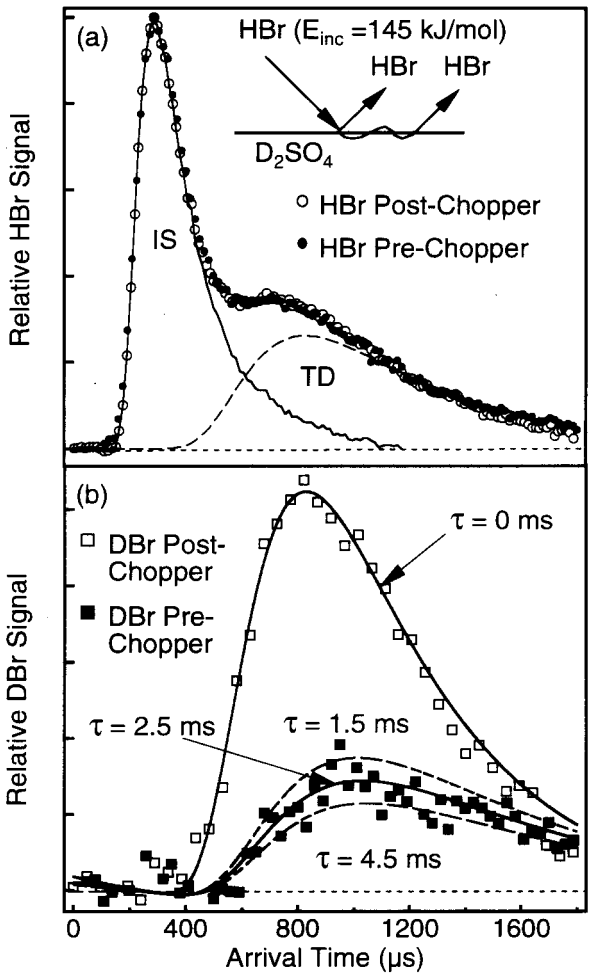


**Figure 8.** Comparison of post- and pre-chopper spectra for HBr and DBr after HBr collisions with 68.6 wt % $D_2SO_4$ at 213 K. (a) Post and pre-chopper spectra for HBr. The identical TD signals indicate that the residence time for unexchanged HBr is less than 2 $\mu$s. (b) Post and pre-chopper spectra for H → D exchanged DBr. The best-fit residence time, $\tau_{DBr}$, is 2.5 (+2.0, −1.0) ms.

HCl beam results in a higher degree of HCl thermalization but the pre- and post-chopper spectra remain identical.

The spectra in Figure 8b correspond to DBr molecules that desorb from the acid after H → D exchange. In contrast to the HBr spectra in the top panel, the intensity of the DBr pre-chopper spectrum is significantly lower and shifted to longer arrival times relative to the corresponding post-chopper DBr spectrum. This broadening is attributed to the distribution of residence times of HBr in the acid.

The pre-chopper spectrum can be simulated by weighting a series of time-shifted Maxwell−Boltzmann distributions, $N_{MB}(t)$, with the probability $p_{des}(t_{res})$ that molecules in the incident gas pulse desorb from the acid at a time $t_{res}$ later. The overall fit to the data, $N_{fit}(t_{arrival})$, is given by the convolution

$$N_{fit}(t_{arrival}) = \int_0^{t_{arrival}} p_{des}(t_{arrival} - t)\, N_{MB}(t)\, dt \qquad (1)$$

The weighting coefficient $p_{des}(t_{res} = t_{arrival} - t)$ depends on the characteristic residence or solvation time, $\tau$, of the gas molecules dissolved in the acid. This characteristic residence time is predicted by solution−diffusion models to be[21,39]

$$\tau = D(4H^*RT_{acid}/\alpha_{th}\langle v\rangle)^2 \qquad (2)$$

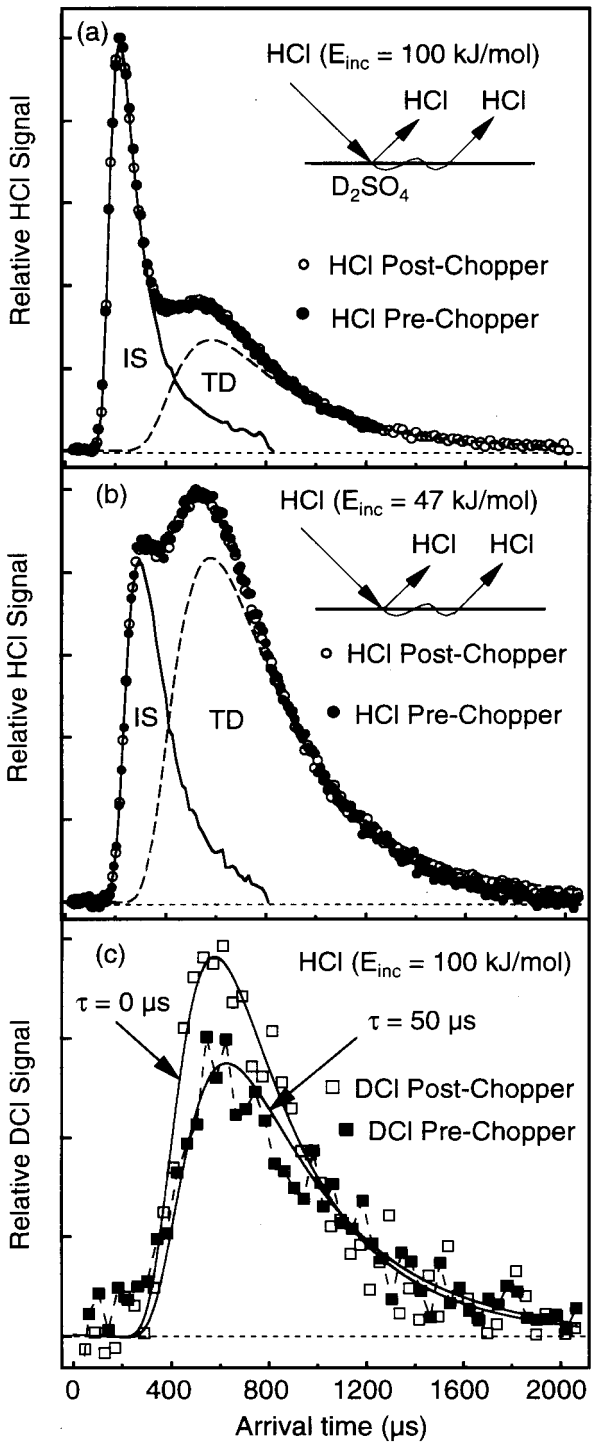


**Figure 9.** Panels a and b show the post- and pre-chopper spectra for HCl and DCl after HCl collisions with 68.6 wt % $D_2SO_4$ collisions at $E_{inc}$(HCl) = 100 and 47 kJ/mol, respectively. The identical pre- and post- signals indicate that the residence time for unexchanged HCl is less than 2 $\mu$s. (c) Post and pre-chopper spectra for desorbing DCl. The best-fit residence time, $\tau_{HCl}$, is approximately 50 $\mu$s.

where $D$ is the solute diffusion coefficient in the acid, $\langle v\rangle$ is the average gas velocity of thermally desorbing DX, $H^*$ is the solubility of all X-containing species, and $\alpha_{th}$ is the fraction of thermally impinging HX molecules that enter the acid. The time $\tau$ is equal to the time required for the rate of gas molecules leaving the acid to rise to 57% of its final rate, as the initially fresh liquid becomes saturated with gas and the desorption flux approaches its maximum value. The calculation of $p_{des}$ for our experimental conditions is described in the Appendix.

Simulations of the DBr pre-chopper TOF spectrum are shown by the solid and dashed curves in Figure 8b. The post-chopper spectrum is fit by a Maxwell−Boltzmann distribution (for which $\tau = 0$), as the arrival times depend only on exit velocities and not on residence times. The pre-chopper simulations for $\tau > 0$ show that finite residence times broaden and shift the desorption distribution to longer arrival times and, even more noticeably, lower the peak intensities relative to those of the post-chopper curve. The drop in intensity is due to molecules that diffuse deeply into the acid and emerge at later times, spreading the signal over arrival times beyond the 2000-$\mu$s limit of the TOF spectrum. We find that the shape and intensity of the pre-chopper DBr spectrum of Figure 8b are simultaneously best fit by a residence time of $\tau = 2.5\ (+2.0, -1.0) \times 10^{-3}$ s. As the simulations at different values of $\tau$ show, the fits are more sensitive to changes in intensity than to shifts in time. The predicted curves emphasize the distinction between the residence time $\tau$ of 2.5 ms, which characterizes the entire desorption distribution, and the smaller shift in peak arrival time of 0.2 ms. The observed 2.5-ms residence time is in good agreement with the 2-ms value predicted by eq 2.[40,41] The observed residence times for HBr and DBr demonstrate the large separation in time scales between the trapping−desorption ($<10^{-6}$ s) and trapping−reaction−desorption ($10^{-3}$ s) pathways.

DCl pre- and post-chopper spectra are shown in Figure 9c for HCl collisions with 68.6 wt % $D_2SO_4$. The DCl pre-chopper spectrum is lower in intensity and slightly broader in time than the DCl post-chopper spectrum. Fits to the spectra yield an approximate residence time of 50 $\mu$s. Five separate measurements confirm the reduced intensity of the pre-chopper spectrum, but the low 0.11 H → D exchange fraction and the sensitive dependence of the pre-chopper spectrum on acid concentration make it difficult to reproduce the intensity and background levels precisely. The $5 \times 10^{-5}$ s residence time is shorter than the $3 \times 10^{-3}$ s time for HBr, reflecting the lower solubility of HCl in concentrated sulfuric acid. However, as discussed later, the HCl residence time is longer than that predicted by eq 2 using a solubility based on HCl ionization.

The pre- and post-chopper spectra for nitric acid are shown in Figure 10, recorded at the most intense ion fragment of $m/e = 46$ ($NO_2^+$). Because of dissociative ionization of the parent molecules in the mass spectrometer, the $NO_2^+$ signal is much stronger than the $HNO_3^+$ or $DNO_3^+$ parent ion signals. $HNO_3$ and $DNO_3$ cannot be distinguished at the $NO_2^+$ mass, but the spectra in Figure 6 recorded at the parent masses demonstrate that nearly all thermally desorbing nitric acid molecules are H → D exchanged $DNO_3$ and that all inelastically scattering molecules are reagent $HNO_3$. The $NO_2^+$ post-chopper spectrum in Figure 10, therefore, includes both inelastically scattered $HNO_3$ (for which $<\Delta E_{IS}>/E_{inc} = 0.85$) and thermally desorbing $DNO_3$. In contrast, the thermal-desorption component is almost completely removed from the pre-chopper spectrum. The residence times for $DNO_3$ must be very long, broadening and shifting the pre-chopper TD component by such a large extent that it becomes uncorrelated with the incident pulse and merges with the overall background of the TOF spectrum.

The long residence times for nitric acid can be measured by recording post-chopper spectra at different exposure times, $t_{exp}$, as determined by the rotation speed of the acid-covered wheel.[9] Molecules residing in the liquid for times less than $t_{exp}$ will desorb and reach the mass spectrometer, whereas those undergoing solvation for times longer than $t_{exp}$ will remain dissolved in the acid. As the acid-covered wheel is rotated at slower speeds and $t_{exp}$ is increased, more desorbing gas molecules will be detected, and the TD signal will increase. Figure 11 shows post-chopper TOF spectra for $HNO_3$ at exposure times of 0.078, 0.15, and 0.46 s. The ratio of thermal desorption signals at $t_{exp} =$ 0.078 and 0.46 s is $0.64 \pm 0.03$. As described in the Appendix, this increase in desorption intensity can be modeled with a characteristic residence time of $\tau = 0.10 \pm 0.05$ s. This residence time is close to the 0.2-s time predicted by eq 2.[42]

We can return to Figure 10 and use the 0.1-s residence time to determine the origin of the weak signal at long arrival times in the pre-chopper spectrum. This signal must arise either from thermally desorbing reagent $HNO_3$ molecules that have not reacted or from H → D exchanged $DNO_3$. For $\tau = 0.1$ s, eq 1 generates a pre-chopper desorption spectrum for $DNO_3$ represented by the long-dashed line, which is slightly larger than the shoulder itself. This fit suggests that there is little thermal

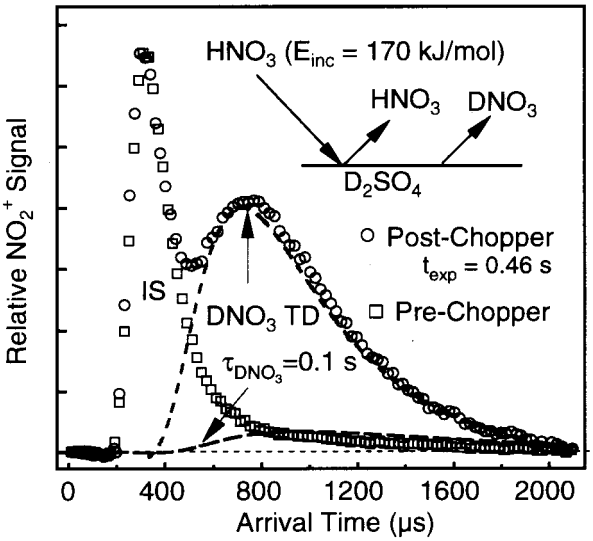


**Figure 10.** Post- and pre-chopper spectra recorded at $NO_2^+$ for $HNO_3$ scattering from 70.5 wt % $D_2SO_4$. The post- and pre-chopper IS signals belong to directly scattered $HNO_3$. The post-chopper TD signal is nearly all H → D exchanged $DNO_3$. The $DNO_3$ molecules desorb so slowly that they are missing from the pre-chopper spectrum. The long-dashed fit to the component at long arrival times in the pre-chopper spectrum is the predicted desorption signal for $\tau = 0.1$ s.

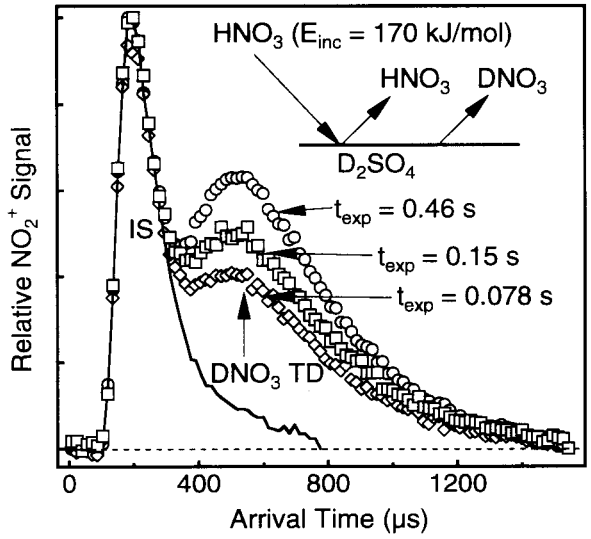


**Figure 11.** Post-chopper spectra for $HNO_3$ scattering from 70.5 wt % $D_2SO_4$ recorded at $NO_2^+$ at three different exposure times, $t_{exp}$. The TD intensity ratios are best fit with $\tau_{DNO_3} = 0.10 \pm 0.05$ s.

desorption of unexchanged $HNO_3$. The absence of signal that can be assigned to $HNO_3$ supports the analysis of Figure 6 that nearly all $HNO_3$ molecules that accommodate in the interfacial region undergo proton exchange before desorbing.

## Discussion

We have used molecular beam scattering of HCl, HBr, and $HNO_3$ from ~70 wt % $D_2SO_4$ at 213 K to investigate the mechanisms of HX trapping, solvation, reaction, and desorption. Our results are four-fold: (1) impinging HX molecules transfer their excess energy efficiently to interfacial $D_2O$ and $D_2SO_4$ molecules and thermalize readily; (2) the fractions of thermally accommodated HX molecules that undergo H → D exchange are $0.11 \pm 0.03$ (HCl), $0.22 \pm 0.03$ (HBr), and $>0.95$ ($HNO_3$), independent of HX collision energy; (3) the residence times for HCl and HBr molecules that do not react are less than 2 $\mu$s, the lower time limit of our experiments; and (4) the estimated residence times for HX molecules that emerge from the acid as DX vary from $5 \times 10^{-5}$ s for HCl and $3 \times 10^{-3}$ s for HBr to $1 \times 10^{-1}$ s for $HNO_3$. In the sections below, we use these results to explore the competition between HX scattering and thermalization and between desorption and reaction of the trapped species.

**HX−Acid Energy Transfer.** The extent of energy transfer in the initial impulsive impact can be investigated by analyzing the energy distributions of those molecules that scatter back into the gas phase before they reach thermal equilibrium with the surface. Table 3 lists the average fractional energy transfers, $\langle \Delta E_{IS} \rangle / E_{inc}$, and the normalized widths of the recoil energy distributions, $\pm \sigma_{IS}/E_{inc}$, for the directly scattered species.

The fractional energy transfers for molecules that scatter inelastically from the acid are extensive for every gas studied, typically exceeding 70%. These large energy transfers reflect the kinematics of collisions between HX molecules and surface $D_2O$ and $D_2SO_4$; the masses of the HX gases exceed the mass of $D_2O$ and are greater than $^1/_3$ the mass of $D_2SO_4$, enforcing substantial momentum transfer upon impact.[43] In addition, we find that the widths of the energy distributions range from 20 to 30% of $E_{inc}$, generating the broad distributions shown in Figures 3b and 4b for HCl and HBr, respectively. The large spreads in final energies are likely due to the different orientations and packing of surface $D_2O$ and $D_2SO_4$ and their thermal motions, as well as multiple HX collisions imposed by surface corrugation.

We can gain more insight by comparing HCl and argon scattering from the acid. Ar is similar to HCl in both size and mass, but because it is atomic and weakly polarizable, collisional energy transfer will be governed by repulsive interactions with surface species and not by internal excitation or long-range attractive forces. The HCl and Ar spectra in Figures 3 and 7 show that, on average, HCl transfers only 5% (or 5 kJ/mol) more of its incident energy than does Ar to the acid. The widths of the energy distributions are also only slightly broader for HCl. Table 3 indicates that HBr and Kr behave similarly. These observations are in accord with calculations of Ar and HCl scattering from water-ice, which show that energy transfer is extensive but that translational energy is not coupled effectively into H−Cl vibrations.[44,45] The similar Ar and HCl scattering distributions suggest that most of the HCl collision energy is transferred initially into motions of surface $D_2O$ and $D_2SO_4$ and not into HCl vibration or rotation and that there are no strong long-range forces initially accelerating HCl into the surface.[46] As Table 3 shows, the fractional energy transfer is greater for $HNO_3$ than for the other gases. This larger value of 0.85 may arise from the higher incident energy employed,[32] as well as from excitation of low-frequency $HNO_3$ torsional modes.

**Thermalization and H → D Exchange.** The large energy transfers in the inelastic channel are accompanied by significant HX thermalization and desorption of HX or DX, as shown in Figures 3−6. The observations of energy-independent proton exchange and thermal desorption of product DX appear to be most consistent with a two-step process in which HX first thermally equilibrates in the interfacial region and then reacts.[36] Figures 3−5 show that, although the IS channel diminishes at lower collision energies, the 9:1 HCl:DCl and 3.5:1 HBr:DBr desorption ratios remain constant. The H → D exchange fractions, therefore, do not depend on the incident energy of HCl over the range of 14−100 kJ/mol, implying that the molecules dissipate their excess energy and lose memory of their initial trajectory before proton exchange occurs. The invariance of $f_{exch}$ with incident energy also argues against gas entry by ballistic penetration of HX through the interface, as this process should drop sharply at lower impact energies. The absence of scattered DX molecules at high velocities further shows that there is no direct H → D exchange that bypasses the thermal equilibration step.

The two-step exchange process allows the exchange probability to be written as a product of the trapping probability and the fraction of trapped molecules that undergo exchange, specifically, $p_{exch}(E_{inc},\theta_{inc}) = p_{trap}(E_{inc},\theta_{inc})f_{exch}$. Within this picture, the exchange rate depends on the molecule's incident trajectory only through changes in the trapping probability with impact energy and angle. Most of our experiments are carried out at incident energies that greatly exceed the average energy of collisions in the stratosphere of $2RT_{acid} = 3.5$ kJ/mol at 213 K. We use energies greater than 100 kJ/mol to increase signal levels and to provide a wider separation in arrival times between the IS and TD channels. Even at these high impact energies, however, trapping can occur frequently. Separate studies of HCl collisions with liquid glycerol show that $p_{trap}$ is 0.6 at $E_{inc}$ =100 kJ/mol and $\theta_{inc} = 45°$.[38] This value rises to 0.9 at $E_{inc} = 14$ kJ/mol as trapping becomes more probable at lower impact energies[36,47] where there is less energy to dissipate before the molecule becomes bound in the attractive gas−surface potential.[43,48] HCl scattering from water-ice further shows that $p_{trap}$ is greater than 0.9 at 100 K and $E_{inc} = 9$ kJ/mol.[49,50]

We also infer high values of $p_{trap}$ for HCl collisions with 70 wt % $D_2SO_4$. Figure 5b implies that $p_{trap}$ must be near 1 at $E_{inc} = 14$ kJ/mol in order for the IS:TD ratio to be smaller than 0.1. When the relative DCl desorption signals at $E_{inc} = 14$ and 100 kJ/mol are normalized by the HCl incident beam intensities, the trapping probability at 100 kJ/mol is found to be roughly 50% of the value at 14 kJ/mol, indicating that many HCl molecules fully dissipate their excess energy into the acid even at high collision energies.

**Competition between HX Desorption and H → D Exchange.** *HCl Desorption and Exchange*. Although HCl thermalizes readily at the surface of 70 wt % $D_2SO_4$, the attractive forces between HCl and interfacial $D_2O$ and $D_2SO_4$ do not appear to be sufficiently strong to bind most HCl molecules long enough to allow them to undergo proton exchange. Our measurements show that $f_{exch}$ is only $0.11 \pm 0.03$ for HCl, indicating that nearly 90% of the thermalized HCl molecules desorb from the acid, dissipating their collision energy but escaping before they dissociate into $H^+$ and $Cl^-$ or undergo other reactions.

The values of $f_{exch}$ should be expressible in terms of a competition between the reaction and desorption of HX species trapped in the interfacial region of the acid, assuming that all thermalized molecules become bound (trapped) at the surface before desorbing or reacting. Specifically, the ratio of DX to HX thermal desorption intensities is the ratio of rates for reaction and desorption of trapped HX molecules, allowing the exchange fraction to be written as $f_{exch} \equiv TD(DX)/[TD(DX) + TD(HX)] = k_{exch}/(k_{exch} + k_{des})$ and the exchange probability to be written as

$$p_{exch} = p_{trap} f_{exch} = p_{trap} k_{exch}/(k_{exch} + k_{des}) \qquad (3)$$

where $k_{des}$ is the rate constant for HX desorption averaged over all adsorption sites and $k_{exch}$ is the rate constant for H → D exchange, encompassing both interfacial and solution phase solvation and reaction. Equation 3 may be compared with the expression for the mass-accommodation coefficient, $\alpha_{th}$, as developed by Worsnop et al.[51,52] and by Hanson[53]

$$\alpha_{th} = p_{trap} k_{sol}/(k_{sol} + k_{des}) \qquad (4)$$

where $k_{sol}$ is the rate constant for transport of thermalized molecules through the interface and into solution. As discussed below, the residence time measurements indicate that HX molecules that undergo H → D exchange spend time as neutral or ionic species in the bulk region of the acid, whereas those that do not exchange do not appear to enter the acid. When reaction occurs after bulk solvation, these observations imply that $k_{sol}$ and $k_{exch}$ should be nearly equal and thus that $\alpha_{th}$ is nearly equal to $p_{exch}$. Additionally, $p_{trap}$ should be close to 1 at thermal collision energies, further implying that $\alpha_{th}$ is approximately equal to $f_{exch}$.

Equations 3 and 4 show that either high desorption rate constants or low exchange/solvation rate constants result in limited reactive uptake of HX molecules into the acid. From a value of $f_{exch}(HCl) = 0.11$, the desorption rate constant for HCl is inferred to be eight times higher than the exchange/solvation rate constant. It appears that the residence times for most HCl molecules are insufficient for solvating the trapped molecules before they are kicked away from the surface by thermal motions of the interfacial molecules, enforcing low probabilities for HCl mass accommodation and reaction.

The distinct time scales for trapping−desorption and trapping−reaction−desorption are supported by residence time measurements of HCl and DCl in contact with the acid. Figure 9 shows that HCl molecules that do not undergo proton exchange must desorb in less than 2 $\mu$s. These molecules may remain in the interfacial region of the acid during this time period or they may begin to diffuse into solution. An average diffusion depth (beyond rapid penetration through the top one or two lower-density monolayers) can be estimated from $(D\tau)^{1/2} \approx 10$ Å, assuming that $\tau$ is $2 \times 10^{-6}$ s and the solute diffusion constant $D$ is $5 \times 10^{-9}$ cm$^2$/s.[54,55] This estimate of the depth is an upper bound, limited by the 2-$\mu$s time resolution of the prechopper experiments, and the actual contact time and penetration depth may be much smaller. If the trapped HCl molecules remain at the surface of the acid before they desorb, their residence times will be governed by bonding to surface molecules rather than by diffusion. Hydrogen bonding between HCl and surface OD and SO groups should provide the strongest bonds, but other configurations involving different dipolar or dispersion interactions may also bind HCl to the surface during its contact time with the acid. Judging from a computed adsorption energy of 10 kJ/mol for argon on water-ice,[44] we would expect that the attractive potential for most HCl−acid configurations to be equal to or greater than this value. This adsorption energy exceeds $5RT_{acid}$, implying that even thermalized HCl molecules that do not hydrogen bond to surface $D_2O$ or $D_2SO_4$ will be trapped momentarily at the interface.[44,48]

The most pertinent information for hydrogen bonding of HCl to the surface of sulfuric acid may come from studies of HCl adsorption at the surface of amorphous ice and solid $HCl{\cdot}6H_2O$, extrapolated to 213 K.[49,56−60] The adsorption energy and prefactor measured by Isakson and Sitz of $E_{ads} = 28$ kJ/mol and $\tau^0_{surf} = 5 \times 10^{-15}$ s predict an HCl surface residence time of $\tau_{surf} = \tau^0_{surf} \exp(E_{ads}/RT_{acid}) = 4 \times 10^{-8}$ s at 213 K.[49] The parameters of Graham and Roberts of $E_{ads} = 28-38$ kJ/mol and $\tau^0_{surf} = 1 \times 10^{-13}$ s predict $\tau_{surf} = 7 \times 10^{-7}$ to $2 \times 10^{-4}$ s.[56] HCl residence times based on $E_{ads} = 28$ kJ/mol are shorter than our measured lower limit of $2 \times 10^{-6}$ s, making it plausible that hydrogen-bonded HCl can desorb within 2 $\mu$s from the surface of aqueous sulfuric acid at 213 K. We note that Graham and Roberts observed that HCl molecules adsorbed on solid $DCl{\cdot}6D_2O$ undergo only 40% H → D exchange before desorbing at 140 K, indicating that molecularly bound HCl has limited pathways for proton transfer at the surface of the solid hexadeuterate.[56,60]

Our experiments show that HCl−surface interaction times of $2 \times 10^{-6}$ s or less prohibit ~90% of the thermalized HCl from reacting with 70 wt % $D_2SO_4$ before they desorb. The 11% that do react may be among those molecules that persist on the surface long enough for surface $D_2O$ and $D_2SO_4$ to reorganize and surround the HCl, solvating it sufficiently for dissociation or other reactions to occur either immediately or deeper within the acid.[61,62] The average lifetime of reacting HCl molecules can be estimated from the pulsed-beam spectrum in Figure 9c of DCl desorbing from 68.6 wt % $D_2SO_4$. The $\sim 5 \times 10^{-5}$ s characteristic residence time is much longer than the trapping−desorption time of $< 2 \times 10^{-6}$ s. This long residence time indicates that DCl is not produced solely by interfacial exchange and desorption but by a process that is accompanied by dissolution deeper into the acid. The measured residence time is also longer than the submicrosecond time predicted by eq 2,[63] based on an HCl solubility involving $Cl^-$ and HCl species.[17] Robinson et al. recently postulated that HCl dissolution may involve formation of chlorosulfonic acid,[6] perhaps through reaction of HCl with $HSO_4^-$ and $H^+$. The lifetime of the $ClSO_3D$ product in 68.6 wt % $D_2SO_4$ is limited by the observed uptake of $0.01 \pm 0.02$ measured at $^{35}Cl$, which indicates that nearly all Cl-containing species evaporate from solution within the exposure time of 0.46 s. The $ClSO_3D$ must, therefore, desorb from the acid or decompose into DCl that desorbs during this exposure time. $ClSO_3H$ is more acidic than $H_2SO_4$ and should be present mostly in its ionic form, $ClSO_3^-$,[64] making it likely that the desorbing chlorine species is DCl, regenerated from $ClSO_3^- + D_3O^+$. We could find no evidence for molecular $ClSO_3D$ in the gas phase monitored at $ClSO_3D^+$ or $SO_3^+$, further suggesting that any $ClSO_3D$ formed in solution decomposes before it desorbs.

Within the picture outlined above, H → D exchange involves HCl adsorption and solvation for times longer than 2 $\mu$s, either concurrent with or followed by HCl dissociation and DCl recombination in conjunction with the formation and decomposition of chlorosulfonic acid. Judging from an overall residence time of 50 $\mu$s, the solvated HCl, $Cl^-$, $ClSO_3^-$, and DCl must together diffuse through a distance of $(D\tau)^{1/2} \approx 50$ Å before DCl desorbs from the acid.

*HBr Desorption and Exchange*. HBr is ~100 times more acidic than HCl[23] and ~200 times more soluble in 70 wt % sulfuric acid,[17] yet it exchanges only twice as often with the acid. The pre-chopper measurements reveal that, like HCl, the parent HBr molecules that equilibrate in the interfacial region spend less than ~2 $\mu$s in contact with the acid before desorbing back into the gas phase. The low proton exchange fraction of 0.22 yields $k_{des} \approx 3.5k_{exch}$, indicating that the short residence time is typically less than that required for HBr to react.

Figure 8b shows that the HBr molecules that do undergo exchange follow a process that can be modeled well by a residence time of 2.5 ms, roughly fifty times longer than that of HCl. The mechanism for H → D exchange must therefore involve a relatively stable and soluble intermediate. Judging from the large acid dissociation constant for HBr and the instability of $BrSO_3H$,[65] we expect HBr to dissociate into $H^+$ and $Br^-$ once the parent molecule is sufficiently solvated in the near-interfacial region of the acid.[62] The solvated $Br^-$ ions can then diffuse deeper into the bulk, remaining there for an average of 2.5 ms before migrating near the surface and recombining with $D^+$ to produce desorbing DBr.

The probability that a thermally equilibrated HBr or HCl molecule undergoes H → D exchange is likely governed by the hydrogen bonding strengths for HX to surface $D_2O$ and $D_2SO_4$ and by the solvation requirements for HX dissociation in the near-interfacial region of the acid. Quantum calculations indicate that the ~19 kJ/mol hydrogen bond in $HCl-H_2O$ is slightly stronger than that in $HBr-H_2O$.[24,25] This ordering suggests that HCl should remain in contact with the surface longer than HBr. However, HBr is a stronger acid than HCl in pure water,[23] and it dissolves more exothermically in concentrated sulfuric acid.[17] Quantum calculations also predict that the minimum number of water molecules required for dissociation of HBr in $HBr(H_2O)_n$ is three, which is one water molecule less than for HCl.[24,25,28,66] $f_{exch}$ may therefore be higher for HBr because fewer solvent molecules are required to stabilize $H^+-Br^-$ than $H^+-Cl^-$, allowing dissociation to compete more effectively with hydrogen bond breaking and HX desorption.

*$HNO_3$ Desorption and Exchange*. In contrast to HCl and HBr, $HNO_3$ undergoes nearly complete proton exchange in collisions with 70.5 wt % $D_2SO_4$. Figure 6 indicates that 5% or fewer of the $HNO_3$ that thermally equilibrate with sulfuric acid can escape without reacting; nearly all nitric acid molecules that survive a collision with the acid are those that scatter inelastically.

The efficient H → D exchange may proceed through nitric acid dissociation and recombination with solvent $D^+$ or, alternatively, by a cyclic, concerted H and D transfer between neutral $HNO_3$ and $DSO_4^-$. A third pathway involving $HNO_3$ deuteration and deprotonation, $HNO_3 + D^+ \rightarrow [DHNO_3^+ \leftrightarrow HOD + NO_2^+] \rightarrow H^+ + DNO_3$, is less probable, based on Raman measurements that show that $HNO_3$ acts like a weak acid in 72 wt % $H_2SO_4$ at 25 °C, in which it is 97% molecular $HNO_3$and 3% $NO_3^-$.[22] Despite its nonionic form, nitric acid interacts strongly enough with bulk $D_2O$, $D_3O^+$, and $DSO_4^-$ to remain within 70.5 wt % $D_2SO_4$ for 0.1 s on average. This measured residence time reflects the enormous solubility of $>10^6$ M/atm and high solvation enthalpy for molecular $HNO_3$ in the acid.

The multiple hydrogen bonds that promote the very exothermic and long-time solvation of $HNO_3$ within the bulk acid are also expected to be strong at the surface. Quantum calculations predict that the $HNO_3-H_2O$ and $HNO_3-H_2SO_4$ dissociation energies are 31 and 43 kJ/mol,[26,29] at least 60% greater than that for the analogous HCl complexes. These higher binding energies should lead to $HNO_3$ residence times at the acid surface that are many times longer than those for HCl or HBr. In contrast, $HNO_3$ is a much weaker acid than HCl or HBr and may require more solvent molecules to bring about dissociation in 70 wt % $D_2SO_4$.[67] Any requirement for more extensive solvation, however, appears to be outweighed by the ability of $HNO_3$ to form strong hydrogen bonds: the observed value of $f_{exch} > 0.95$ implies that the interfacial residence time is long enough for the acid to capture nearly every $HNO_3$ molecule that thermalizes during a collision.

## Summary and Conclusions

Molecular beam studies of HCl, HBr, and $HNO_3$ collisions with 70 wt % $D_2SO_4$ help to elucidate the pathways for HX thermalization, H → D exchange, and DX desorption. We find that energy transfer is extensive for all three HX molecules, exceeding 70% of the impact energy. The similar inelastic scattering distributions for HCl and Ar (and for HBr and Kr) suggest that most of the incident energy is dissipated initially into motions of surface $D_2O$ and $D_2SO_4$ and not into HCl or HBr rotational or vibrational motions. The large energy transfers and the weak inelastic signals at low $E_{inc}$ imply that the trapping probabilities rise as the incident energy is decreased and probably approach 1 at thermal impact energies.

The subsequent fate of the thermally equilibrated HX molecules is governed by the competition between the rate of desorption and the rate of interfacial and bulk solvation and dissociation. Only 11% and 22% of the thermalized HCl and HBr molecules, respectively, undergo H → D exchange before they are propelled from the interface by thermal motions of surface $D_2O$ and $D_2SO_4$. In contrast, greater than 95% of the trapped $HNO_3$ molecules are converted to $DNO_3$ before they desorb. Residence time measurements show that the HCl and HBr molecules that do not undergo proton exchange must desorb from the interface within 2 $\mu$s, the lower time limit of our experiments.

HX molecules that undergo H → D exchange in 70 wt % $D_2SO_4$ spend longer than 2 $\mu$s in contact with the acid. The observed solvation times scale with the HX solution-phase solubility and exothermicity.[4,6,17,19-21] The $\sim 5 \times 10^{-5}$ s characteristic residence time for HCl indicates that exchange typically occurs within the outer 50 Å of the acid, and it supports the hypothesis of Robinson et al. that the solubility of HCl may be driven by direct reactions of HCl with solvent acid species as well as by dissociation.[6] Trapped HBr molecules are likely to dissociate even closer to the interface,[62] but the resulting $Br^-$ ions are much more stable than the $Cl^-$ ions and are found to reside in the acid for a characteristic time of $3 \times 10^{-3}$ s before diffusing to the surface and recombining with solvent $D^+$. The $1 \times 10^{-1}$ s residence time for $HNO_3$ in 70.5 wt % $D_2SO_4$ is much greater than that of either HCl or HBr. The high H → D exchange rate and long residence time for $HNO_3$ may be driven by its ability to form strong hydrogen bonds, both to surface $D_2SO_4$ and $D_2O$ and to sulfuric acid species within solution. In contrast, HCl and HBr appear to bind more weakly to interfacial molecules and, therefore, to desorb more quickly from the surface, prohibiting their potentially greater solution acidity from promoting solvation and dissociation within the acid.

The nearly 100% H → D exchange probability for nitric acid and its efficient energy dissipation imply that stratospheric $HNO_3$ should be absorbed into 70 wt % sulfuric acid aerosols at nearly the maximum gas kinetic rate in the stratosphere, whereas the low values of $f_{exch}$ for HCl and HBr imply that they are poor sources of aqueous $Cl^-$ and $Br^-$ ions. In particular,

HCl both is highly insoluble in 70 wt % sulfuric acid and frequently desorbs from the acid's surface before it reacts. The low solubility of HCl in concentrated sulfuric acid is one of the primary reasons for concluding that its reactions with other solute molecules will play a smaller role in the mid-latitude regions than at higher latitudes, where the aerosols are more dilute.[2,3,68] The scattering experiments imply that the reactivity of HCl is even lower than first expected because, in nine collisions out of 10 with 70 wt % sulfuric acid, HCl will desorb from the surface of the aerosol too quickly to react even with the solvent acid itself.

**Acknowledgment.** We are grateful to the Air Force Office of Scientific Research, the Petroleum Research Fund, administered by the American Chemical Society, and the National Science Foundation for funding this research. P.M.B. thanks the Deutsche Forschungs Gemeinshaft for a fellowship. We thank John Fenn and James Taylor for the loan of vacuum and electronic equipment and Edwin Sibert and Arun Yethiraj for advice on numerical calculations of gas uptake. We also appreciate discussions with Fu-Ming Tao, Roberto Bianco, and Simon Clegg concerning HX hydrogen bonding and dissociation and with David Hanson and Douglas Worsnop concerning the uptake process.

## Appendix

This appendix describes the calculation of the desorption probability $p_{des}(t)$ used to determine the characteristic residence time $\tau$ of HX molecules in sulfuric acid. The relative probability, $p_{des}(t) = F_{des}(t)/F_{des}(t\rightarrow\infty)$, is equal to the flux $F_{des}(t)$ of gas molecules desorbing from the liquid at time $t$, divided by the asymptotic outgoing flux $F_{des}(t\rightarrow\infty)$. The desorbing flux is given by $F_{des}(t) = \gamma_{des}(t)F_{beam}$, where $F_{beam}$ is the steady flux of impinging molecules and $\gamma_{des}(t)$ is the desorption coefficient. $p_{des}(t)$ is therefore equal to $\gamma_{des}(t)/\gamma_{des}(t\rightarrow\infty)$ and increases from 0 to 1 as the fresh liquid becomes saturated with gas. $p_{des}(t)$ can also be expressed as

$$1 - \gamma_{uptake}(t)/\gamma_{uptake}(t=0)$$

where $\gamma_{uptake}(t)$ is the net fraction of molecules entering the liquid at time $t$. The desorption probability is calculated from $p_{des}(t) = c(x=0,t)/c(x=0,t\rightarrow\infty)$ by numerical integration of the diffusion equation, $D\,\partial^2c(x,t)/\partial x^2 = \partial c(x,t)/\partial t$, where $c(x,t)$ and $D$ are the liquid-phase concentration and diffusion coefficient of the solute, respectively.[69]

The duration, $t_{pulse}$, of the gas pulse in the pre-chopper spectra is 50−65 $\mu$s, and the pulse is assumed to be square in shape. The number of pulses to which a patch of liquid is exposed is given by $n_{pulse} = t_{exp}/t_{interval}$, where the exposure time, $t_{exp}$, is determined by the rotation speed of the acid-covered wheel and the time between pulses, $t_{interval}$, is determined by the rotation speed of the pre-chopper. For typical values of $t_{exp} = 0.46$ s and $t_{interval} = 0.002$ s, $n_{pulse}$ is 230. Each pulse deposits gas into the liquid, and some molecules will remain in the liquid when the next pulse reaches the surface unless the gas residence time is much shorter than $t_{interval}$. Thus, there is generally a different $p_{des}(t)$ function for each pulse as gas builds up in the liquid. We take this into account by calculating $n_{pulse}$ separate desorption curves and averaging them to generate one desorption function.

Graphs of the average $p_{des}(t)$ function are shown in Figure A.1 for characteristic residence or solvation times $\tau$ of 0, 10, 100, and 1000 $\mu$s. The curves are divided into two regions, labeled "beam on" and "beam off". In the beam-on region between $t = 0$ and $t_{pulse}$, $c(x,t)$ must satisfy the conditions

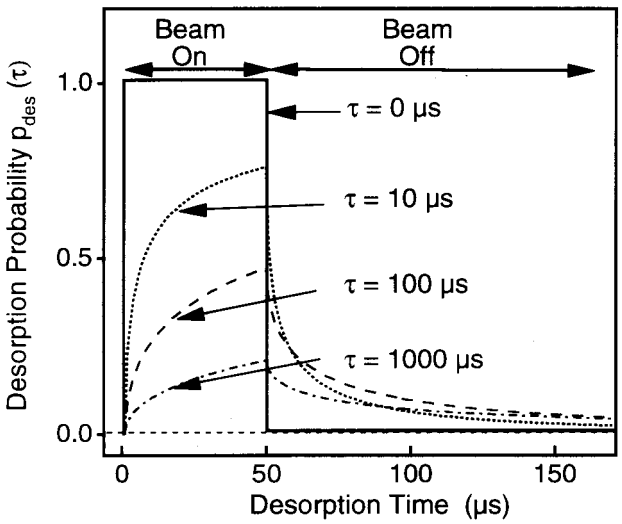


**Figure A.1.** Plot of $p_{des}$ versus desorption time for $\tau = 0$, 10, 100, and 1000 $\mu$s using $t_{exp} = 0.13$ s, $t_{pulse} = 50$ $\mu$s, $t_{interval} = 2000$ $\mu$s, and $n_{pulse} = 65$.

$$c_1(x,t=0) = 0 \text{ for the first gas pulse} \quad \text{(a1)}$$

$$c_i(x,t=0) = c_{i-1}(x,t_{interval}) \text{ for } i = 2 \text{ to } n_{pulse} \quad \text{(a2)}$$

$$c_i(x\rightarrow\infty,t) \rightarrow 0 \quad \text{(b)}$$

$$-D\,\partial c_i(x,t)/\partial x|_{x=0} = F_{in} - F_{des}(t) = [\alpha(E_{inc},\theta_{inc}) - \gamma_{des}(t)]F_{beam} \quad \text{(c)}$$

$$= (D/\tau)^{1/2}[c(x,t\rightarrow\infty) - c_i(x,t)]|_{x=0}$$

Condition a2 sets the initial concentration profile for the $n$th gas pulse equal to the profile just before that pulse reaches the surface. Condition c enforces mass conservation across the gas−liquid interface. The quantity $F_{in} = \alpha(E_{inc},\theta_{inc})\,F_{beam}$ is the flux of molecules entering the liquid from the impinging molecular beam, where $\alpha(E_{inc},\theta_{inc}) = \gamma_{des}(t\rightarrow\infty) = \gamma_{uptake}(t=0)$ is the fraction of molecules that enter the liquid before desorbing. The quantity $(D/\tau)^{1/2}$ is the rate constant for transport through the plane at $x = 0$ dividing the gas and liquid phases, where $\tau$ is given by eq 2.

For the time between $t_{pulse}$ and $t_{interval}$, the gas pulse is off, and the gas deposited earlier by the molecular beam continues to desorb from the liquid, but with no incoming molecules to replenish those that leave. The diffusion equation is solved using the altered boundary condition at $x = 0$ in this beam-off region.

$$-D\,\partial c_i(x,t)/\partial x|_{x=0} = -F_{des}(t) = -\gamma_{des}(t)F_{beam} = -(D/\tau)^{1/2}c_i(x,t)]|_{x=0} \quad \text{(c′)}$$

The diffusion equation is solved numerically to determine $p_{des}(t_{interval} > t > t_{pulse}) = c_i(x=0,t)/c(x=0,t\rightarrow\infty)$ in this region.

The ascending curves in Figure A1 show that, in the beam-on region, $p_{des}(t)$ rises steadily with time as gas molecules enter the acid. After the gas pulse ends at time $t_{pulse}$, $p_{des}(t)$ drops as the molecules desorb and deplete the liquid of gas. The four curves demonstrate that, at longer times $\tau$, the curves rise and fall less sharply, although the total area under each curve remains equal. This smoothing occurs because the gas molecules are more soluble at larger $\tau$ and, therefore, diffuse more deeply and

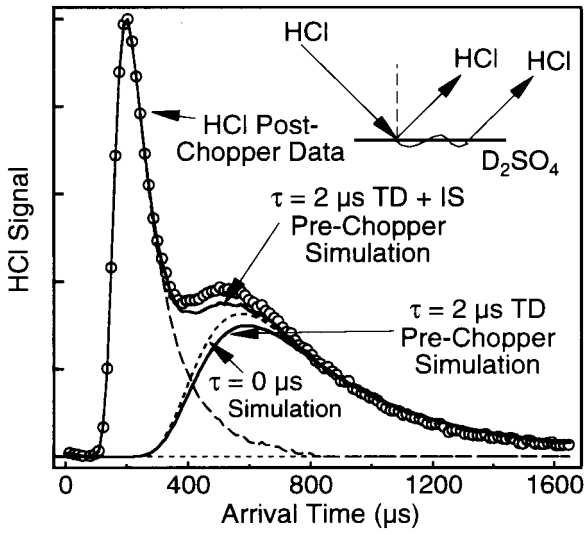


**Figure A.2.** Post- and pre-chopper spectra for HCl, in which the thermal desorption component of the pre-chopper spectrum has been artificially convoluted with $p_{des}(\tau=2\ \mu s)$. The resulting spectrum (solid line) is just distinguishable from the post-chopper ($\tau = 0\ \mu s$) spectrum (circles), indicating that a 2-$\mu$s shift is close to the shortest discernible residence time.

desorb more slowly in both regions. The averaged $p_{des}(t)$ is a function only of the characteristic residence time $\tau$, the pulse width $t_{pulse}$, and the time interval between pulses, $t_{interval}$.

The best-fit thermal distributions, $N_{fit}$, for the pre-chopper spectra in Figures 8−10 are obtained by convoluting $p_{des}$ with a Maxwell−Boltzmann distribution, $N_{MB}$, according to eq 1, where $N_{MB}(t) \sim t^{-4} \exp[-m_{gas}(d_{pre}/t)^2/2RT_{acid}]$. The post-chopper spectrum is then fit with a value of $\tau = 0$ in order to scale the intensities of the pre- and post-chopper data, and the value of $\tau$ for the pre-chopper spectrum is adjusted until both the shape of the pre-chopper spectrum and its relative intensity are reproduced. All fits are corrected for "wrap-around" effects, in which the thermal desorption signal at long times that is cut off at the end of the TOF recording interval is added on to the beginning of the spectrum.

Figure A2 demonstrates how the time and intensity shifts of the pre-chopper spectrum allow measurements of microsecond residence times. The post-chopper spectrum for HCl in Figure 3 is superimposed on a pre-chopper spectrum in which the thermal-desorption component has been artificially convoluted with $p_{des}$ using $\tau = 2\ \mu s$. This short residence time generates a visible reduction in signal intensity even though the shift in arrival time cannot be discerned. From the signal-to-noise levels of our data and our confidence in measuring systematic arrival-time and intensity corrections, we estimate that residence times of 2 $\mu$s or longer can be extracted by analysis of pre- and post-chopper data.

Finally, the ratio of intensities of the thermal-desorption components in the post-chopper spectra in Figure 11 can be simulated if we assume that all desorbing molecules are $DNO_3$. In this case, the ratio of integrated thermal desorption intensities, $TD(t_{exp})$, is given by

$$TD(t_{exp}=0.46\ s)/TD(t_{exp}=0.078\ s) = [(1/0.46)\int_0^{0.46} p_{des}(t)\,dt]/[(1/0.078)\int_0^{0.078} p_{des}(t)\,dt]$$

where $p_{des}(t)$ for the continuous (post-chopper) spectra is equal to $1 - \mathrm{erfc}(\sqrt{t/\tau})e^{t/\tau}$.[21,61] The best-fit value of $\tau$ is 0.10 ± 0.05 s for a ratio of TD intensities of 0.64 ± 0.03. The fraction of $DNO_3$ molecules remaining in the acid at a selected time $t_{exp}$ is equal to $1 - TD(t_{exp})/TD(\infty)$. Using $\tau = 0.10$, we estimate that 36% of the $HNO_3$ molecules that have entered the acid have not desorbed at $t_{exp} = 0.46$ s.

## References and Notes

(1) Fahey, D. W.; Kawa, S. R.; Woodbridge, E. L.; Tin, P.; Wilson, J. C.; Jonsson, H. H.; Dye, J. E.; Baumgardner, D.; Borrmann, S.; Toohey, D. W.; Avallone, L. M.; Proffitt, M. H.; Margitan, J.; Loewenstein, M.; Podolske, J. R.; Salawitch, R. J.; Wofsy, S. C.; Ko, M. K. W.; Anderson, D. E.; Schoeberl, M. R.; Chan, K. R. *Nature* **1993**, *363*, 509. Hanson, D. R.; Ravishankara, A. R.; Solomon, S. *J. Geophys. Res., Atmos.* **1994**, *99*, 3615. Williams, L. R.; Manion, J. A.; Golden, D. M.; Tolbert, M. A. *J. Appl. Meteorol.* **1994**, *33*, 785. Robinson, G. N.; Worsnop, D. R.; Jayne, J. T.; Kolb, C. E.; Davidovits, P. *J. Geophys. Res., Atmos.* **1997**, *102*, 3583.

(2) Carslaw, K. S.; Peter, T.; Clegg, S. L. *Rev. Geophys.* **1997**, *35*, 125.

(3) Hanson, D. R. *J. Phys. Chem. A* **1998**, *102*, 4794. Hanson, D. R.; Ravishankara, A. R. *J. Phys. Chem.* **1994**, *98*, 5728.

(4) Abbatt, J. P. D.; Nowak, J. B. *J. Phys. Chem. A* **1997**, *101*, 2131.

(5) Waschewsky, G. C. G., Abbatt, J. P. D. *J. Phys. Chem. A.* **1999**, *103*, 5312. Donaldson, D. J.; Ravishankara, A. R.; Hanson, D. R. *J. Phys. Chem. A* **1997**, *101*, 4717. Hanson, D. R.; Ravashankara, A. R. *Geophys. Res. Lett.* **1995**, *22*, 385. Zhang, R. Y.; Leu, M. T.; Keyser, L. F. *J. Phys. Chem.* **1994**, *98*, 13563.

(6) Robinson, G. N.; Worsnop, D. R.; Jayne, J. T.; Kolb, C. E.; Swartz, E.; Davidovits, P. *J. Geophys. Res., Atmos.* **1998**, *103*, 25371.

(7) See also: Zhang, R. Y.; Leu, M. T.; Keyser, L. F. *J. Phys. Chem.* **1996**, *100*, 339. Longfellow, C. A.; Imamura, T.; Ravishankara, A. R.; Hanson, D. R. *J. Phys. Chem. A* **1998**, *102*, 3323.

(8) Molina, M. J.; Zhang, R.; Wooldridge, P. J.; McMahon, J. R.; Kim, J. E.; Chang, H. Y.; Beyer, K. D. *Science* **1993**, *261*, 1418. Tolbert, M. A. *Science* **1994**, *264*, 527.

(9) Klassen, J. K.; Fiehrer, K. M.; Nathanson, G. M. *J. Phys. Chem. B* **1997**, *101*, 9098.

(10) Radüge, C.; Pflumio, V.; Shen, Y. R. *Chem. Phys. Lett.* **1997**, *274*, 140.

(11) Baldelli, S.; Schnitzer, C.; Schultz, M. J.; Campbell, D. J. *J. Phys. Chem. B* **1997**, *101*, 10435. Schnitzer, C.; Baldelli, S.; Shultz, M. J. *Chem. Phys. Lett.* **1999**, *313*, 416.

(12) Fairbrother, D. H.; Johnston, H.; Somorjai, G. *J. Phys. Chem.* **1996**, *100*, 13696.

(13) Williams, L. R.; Long, F. S. *J. Phys. Chem.* **1995**, *99*, 3748.

(14) Zhang, R.; Wooldridge, P. J.; Abbatt, J. P. D.; Molina, M. J. *J. Phys. Chem.* **1993**, *97*, 7351.

(15) Sierra, J.; Ojeda, M.; Wyatt, P. A. H. *J. Chem. Soc.* **1970**, 1570.

(16) Zarahkani N. G.; Vinnik, M. I. *Russ. J. Phys. Chem.* **1963**, *37*, 260. Chen, H.; Irish, D. E. *J. Phys. Chem.* **1971**, *75*, 2672. Young, T. F.; Walrafen, G. E. *Faraday Trans.* **1961**, *57*, 34.

(17) Carslaw, K. S.; Clegg, S. L.; Brimblecombe, P. *J. Phys. Chem.* **1995**, *99*, 11557. Calculations from the aerosol inorganics model available at www.me.udel.edu/wexler/aim.html.

(18) Lietzke, M. H.; Stoughton, R. W. *J. Phys. Chem.* **1963**, *67*, 652.

(19) Zhang, R. Y.; Wooldridge, P. J.; Molina, M. J. *J. Phys. Chem.* **1993**, *97*, 8541.

(20) Williams, L. R.; Golden, D. M.; Huestis, D. L. *J. Geophys. Res., Atmos.* **1995**, *100*, 7329.

(21) Hanson, D. R.; Ravishankara, A. R. *J. Phys. Chem.* **1993**, *97*, 12309.

(22) Sampoli, M.; De Santis, A.; Marziano, N. C.; Pinna, F.; Zingales, A. *J. Phys. Chem.* **1985**, *89*, 2864.

(23) McCoubrey, J. C. *Chem. Soc. Rev. Books* **1954**, 743.

(24) Re, S.; Osamura, Y.; Suzuki, Y.; Schaefer, H. F. *J. Chem. Phys.* **1998**, *109*, 973.

(25) Conley, C.; Tao, F.-M. *Chem. Phys. Lett.* **1999**, *301*, 29. The zero-point energy correction is 1.59 kcal/mol.

(26) Tao, F.-M.; Higgins, K.; Klemperer, W.; Nelson, D. D. *Geophys. Res. Lett.* **1996**, *23*, 1797.

(27) Packer, M. J.; Clary, D. C. *J. Phys. Chem.* **1995**, *99*, 14323. Ying, L.; Zhao, X. *J. Phys. Chem. A* **1997**, *101*, 6807.

(28) Xu, S. C. *J. Chem. Phys.* **1999**, *111*, 2242. Tachikawa, M.; Mori, K.; Osamura, Y. *Mol. Phys.* **1999**, *96*, 1207.

(29) Beichert, P.; Schrems, O. *J. Phys. Chem. A* **1998**, *102*, 10540.

(30) Antman, M. D. Ph.D. Thesis, University of Wisconsin, Madison, WI, 1998.

(31) Lednovitch, S. L.; Fenn, J. B. *AICHE J.* **1977**, *23*, 454.

(32) Saecker, M. E.; Nathanson, G. M. *J. Chem. Phys.* **1993**, *99*, 7056.

(33) The mass spectrometer views 0.48-cm-diameter (umbra) and 0.90-cm-diameter (penumbra) regions of the surface at normal incidence.

(34) Weaver, B. D.; Frankl, D. R. *Rev. Sci. Instrum.* **1988**, *59*, 92.

(35) The cylindrical pre-chopper rejects incident molecules with velocities lower than $3 \times 10^4$ cm/s at a chopper frequency of 250 Hz. However, the incident beams have narrow speed distributions and peak at velocities of $10^5$ cm/s or higher.

(36) Fiehrer, K. M., Nathanson, G. M. *J. Am. Chem. Soc.* **1997**, *119*, 251.

(37) Rettner, C. T.; DeLouise, L. A.; Auerbach, D. J. *J. Chem. Phys.* **1986**, *85*, 1131.

(38) Ringeisen, B. R.; Nathanson, G. M., manuscript in preparation.

(39) Dankwerts, P. V. *Gas−Liquid Reactions*; McGraw-Hill: New York, 1970. Worsnop, D. R.; Zahniser, M. S.; Kolb, C. E.; Gardner, J. A.; Watson, L. R.; Van Doren, J. M.; Jayne, J. T.; Davidovits, P. *J. Phys. Chem.* **1989**, *93*, 1159. Jones, R. H.; Olander, D. R.; Siekhaus, W. J.; Schwarz, J. A. *J. Vac. Sci. Technol.* **1972**, 1429.

(40) Using values of $\alpha_{th} \approx f_{exch} \approx 0.22$, $H^* = 4.1 \times 10^4$ M/atm, and $D = 8.1 \times 10^{-9}$ cm$^2$/s for 70.4 wt % $H_2SO_4$ (68.6 wt % $D_2SO_4$).

(41) See also: Abbatt, J. P. D. *J. Geophys. Res., Atmos.* **1995**, *100*, 14009.

(42) Using values of $\alpha_{th} \approx f_{exch} \approx 1$, $H^* = 2.7 \times 10^6$ M/atm, and $D = 3.9 \times 10^{-9}$ cm$^2$/s for 72.2 wt % $H_2SO_4$ (70.5 wt % $D_2SO_4$).

(43) Grimmelmann, E. K.; Tully, J. C.; Cardillo, M. J. *J. Chem. Phys.* **1980**, *72*, 1039.

(44) Bolton, K.; Svanberg, M.; Pettersson, J. B. C. *J. Chem. Phys.* **1999**, *110*, 5380.

(45) Wang, L.; Clary, D. C. *J. Chem. Phys.* **1996**, *104*, 5663.

(46) Benjamin, I.; Wilson, M. A.; Pohorille, A.; Nathanson, G. M. *Chem. Phys. Lett.* **1995**, *243*, 222.

(47) Brown, D. E.; George, S. M.; Huang, C.; Wong, E. K. L.; Rider, K. B.; Smith, R. S.; Kay, B. D. *J. Phys. Chem.* **1996**, *100*, 4988.

(48) Tully, J. C. *Surf. Sci.* **1981**, *111*, 461.

(49) Isakson, M. J.; Sitz, G. O. *J. Phys. Chem. A* **1999**, *103*, 2044.

(50) Rieley, H.; Aslin, H. D.; Haq, S. *J. Chem. Soc., Faraday Trans.* **1995**, *91*, 2349.

(51) Worsnop, D. R.; Zahniser, M. S.; Kolb, C. E.; Gardner, J. A.; Watson, L. R.; Van Doren, J. M.; Davidovits, P. *J. Phys. Chem.* **1989**, *93*, 1159.

(52) Shi, Q.; Davidovits, P.; Jayne, J. T.; Worsnop, D. W.; Kolb, C. E. *J. Phys. Chem. A* **1999**, *103*, 8812.

(53) Hanson, D. R. *J. Phys. Chem. B* **1997**, *101*, 4998.

(54) The diffusion depth is estimated by calculating $\langle z^2(\tau)\rangle = [\int z^2 c(z,\tau)/c^* \, dz]/[\int c(z,\tau)/c^* \, dz] = 1.1D\tau$, where $c(z,\tau)/c^*$ is the concentration profile of the gas in the liquid for initial exposure at $t = 0$. This profile is $c(z,t)/c^* = \mathrm{erfc}[z/(4Dt)^{1/2}] - \exp[z/(D\tau)^{1/2}] \exp(t/\tau) \mathrm{erfc}[(t/\tau)^{1/2} + z/(4Dt)^{1/2}]$, where erfc is the complementary error function.

(55) Klassen, J. K.; Hu, Z.; Williams, L. R. *J. Geophys. Res.* **1998**, *103* (D13), 16197.

(56) Graham, J. D.; Roberts, J. T. *J. Phys. Chem.* **1994**, *98*, 5974.

(57) Clary, D. C.; Wang, L. *J. Chem. Soc., Faraday Trans.* **1997**, *93*, 2763.

(58) Gertner, B. J.; Hynes, J. T. *Faraday Discuss.* **1998**, *110*, 301.

(59) Geiger, F. M.; Hicks, J. M.; de Dios, A. C. *J. Phys. Chem. A* **1998**, *102*, 1514.

(60) Devlin, J. P.; Uras, N.; Rahman, M.; Buch, V. *Isr. J. Chem.* **1999**, *39*, 261.

(61) Shi, Q.; Li, Y. Q.; Davidovits, P.; Jayne, J. T.; Worsnop, D. R.; Mozurkewich, M.; Kolb, C. E. *J. Phys. Chem. B* **1999**, *103*, 2417. Swartz, E.; Shi, Q.; Davidovits, P.; Jayne, J. T.; Worsnop, D. R.; Kolb, C. E. *J. Phys. Chem. A* **1999**, *103*, 8824.

(62) Bianco, R.; Gertner, B. J.; Hynes, J. T. *Ber. Bunsen−Ges. Phys. Chem.* **1998**, *102*, 518.

(63) Using values of $\alpha_{th} \approx f_{exch} \approx 0.11$, $H^* = 2 \times 10^2$ M/atm, and $D = 8 \times 10^{-9}$ cm$^2$/s for 70.4 wt % $H_2SO_4$ (68.6 wt % $D_2SO_4$), eq 2 predicts that $\tau$ is $1 \times 10^{-7}$ s. The measured value of $\tau$ of $5 \times 10^{-5}$ s yields an effective HCl solubility of $4 \times 10^3$ M/atm.

(64) Barr, J.; Gillespie, R. J.; Robinson, E. A. *Can. J. Chem.* **1961**, *39*, 1266.

(65) Schmidt, V. M.; Talsky, G. *Z. Anorg. Allg. Chem.* **1960**, *303*, 211.

(66) Lee, C.; Sosa, C.; Planas, M.; Novoa, J. J. *J. Chem. Phys.* **1996**, *104*, 7081.

(67) Tao, F.-M. California State University, Fullerton, 1999. Private communication.

(68) Hanson, D. R.; Lovejoy, E. R. *J. Phys. Chem.* **1996**, *100*, 6397.

(69) Ringeisen, B. R. Ph.D. thesis, University of Wisconsin, Madison, WI, 1999.